International Journal of Extreme Manufacturing

TOPICAL REVIEW • OPEN ACCESS

Recent progress in additive manufacturing of SiC ceramics: fabrication, challenges and solutions

To cite this article: Piao Qu *et al* 2026 *Int. J. Extrem. Manuf.* **8** 052007

View the article online for updates and enhancements.

You may also like

- SiC whisker reinforced SiC ceramics prepared by gel-casting and reactive melt infiltration
Yiran Lin and Zhaofeng Chen
- *(Invited)* The Evolving SiC Market and Impact on CMP Supply Chain
Robert Rhoades
- Investigating the laser power and trajectory effect on milled surface quality during SiC ceramic processing
Xiaohui Li, Xin Ding and Haixin Gao

This content was downloaded from IP address 15.204.172.39 on 06/11/2026 at 19:36

OPEN ACCESS
IMMT | IOP Publishing
International Journal of Extreme Manufacturing
Int. J. Extrem. Manuf. **8** (2026) 052007 (33pp)
https://doi.org/10.1088/2631-7990/ae767b

Topical Review

Recent progress in additive manufacturing of SiC ceramics: fabrication, challenges and solutions

Piao Qu[1], Muhammad Irfan Hussain[1], Zeyu Ji[1], Chongyu Long[1], Muhammad Hamza[1], Jiangyi Tang[1], Paolo Colombo[2] and Zhangwei Chen[1,*]

[1] Additive Manufacturing Institute, Shenzhen University, Shenzhen 518066, People's Republic of China
[2] Department of Industrial Engineering, University of Padova, Padova 35131, Italy

E-mail: chen@szu.edu.cn

Received 1 November 2025, revised 17 December 2025
Accepted for publication 31 May 2026
Published 6 July 2026

Abstract

Silicon carbide (SiC) ceramics are vital high-performance materials for demanding industries, valued for their superior mechanical strength and tunable thermal and electronic properties. Additive manufacturing (AM) unlocks their potential by addressing fabrication complexity and enabling design freedom. This review provides a comprehensive overview of AM technologies for SiC, offering an in-depth analysis of manufacturing precision, forming sizes, and emerging applications. It highlights how AM produces intricate, structurally controlled SiC components with enhanced properties. The analysis also addresses persistent challenges, including quality control, densification, and scalability. Furthermore, this review critically examines the advantages and limitations of various AM processes for performance optimization, including high-precision fabrication, post-processing, morphological characteristics, densification, and strength of printed parts. Finally, it outlines future perspectives aimed at advancing material performance and fostering sustainable innovation.

Keywords: additive manufacturing, SiC ceramics, post-treatments, mechanical properties, applications

1. Introduction

Manufacturing defect-free, near-net-shaped functionally graded ceramics with spatially varying compositions, tuned morphologies, enhanced properties, and optimized performance through advanced techniques is a challenge. With rapid technological advancement and the growing demand for innovation in materials, high-performance ceramics are crucial for modern technology. Significantly, silicon carbide (SiC) ceramics, known for their hardness, specific strength, excellent thermal stability, high-temperature resistance, and good chemical stability, are widely used in engineering components, aerospace, precision semiconductors, microfluidic heat transfer, nuclear energy, environmental protection, and energy catalysis[1–4] (Figure 1). Currently, the manufacturing of SiC-based structural ceramics primarily follows a "material-first, shaping-later" approach, where bulk or rotational blank parts are produced through material preparation processes and then machined into their final shape. However, the subtractive manufacturing of SiC ceramic faces several challenges due to their high hardness (9.2–9.5 GPa) and low toughness, which

* Author to whom any correspondence should be addressed.

Original content from this work may be used under the terms of the Creative Commons Attribution 4.0 licence. Any further distribution of this work must maintain attribution to the author(s) and the title of the work, journal citation and DOI.

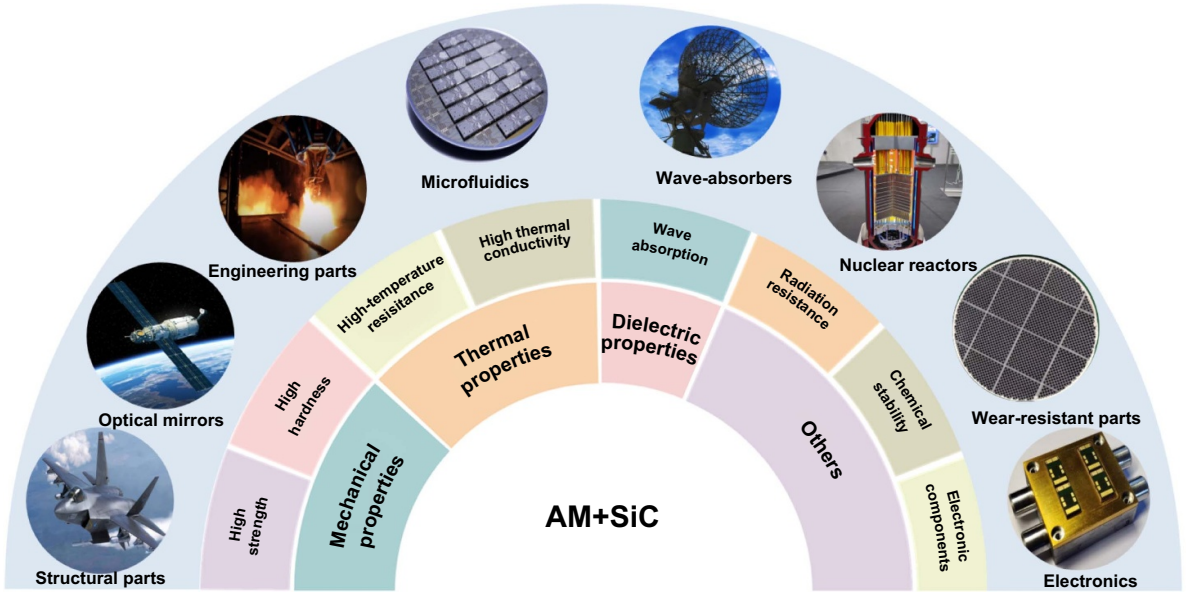


Figure 1. Examples of applications of additively manufactured SiC ceramics in advanced engineering fields.

cause severe tool wear during machining[5]. Additionally, specialized processing techniques such as high-pressure waterjet machining, ultrasonic machining, electrical discharge machining, and laser processing are limited to precision machining of planar surfaces, round holes, and groove structures, making it difficult to fabricate complex-shaped components[6].

Additive manufacturing (AM) provides a novel approach for fabricating SiC structural ceramics. AM techniques, particularly those based on CAD (computer-aided design) models, allow for more precise control over the geometry and microstructure of the final product. Based on the discrete-stacking principle, AM enables the layer-by-layer construction of complex parts, offering high design flexibility[4,7,8]. The "shape control followed by property control" strategy using AM for near-net shaping and sintering to tailor the properties offers a new pathway for manufacturing SiC ceramics with complex geometries. Remarkably, it enables the production of structurally and functionally integrated ceramic components tailored to application needs. Key research in this field focuses on AM processes for SiC-based ceramics, post-sintering treatments, and performance evaluation, which are crucial steps toward practical application. Achieving property-controllable SiC structural ceramics through AM is of significant scientific and technological importance.

To date, various review articles on SiC fabrication techniques can be found in the literature[3,4]. Different from other reviews, the aim of this review is to provide comprehensive knowledge of additive manufacturing techniques, post-processing methods, performance characterization, and material enhancement strategies for SiC ceramics while also examining key challenges in the field. This review is categorized into four major sections: (i) overview of current additive manufacturing techniques used for SiC (e.g., binder jetting, stereolithography, selective laser sintering, and fused deposition modeling). (ii) A summary of post-processing and densification strategies: debinding and pressureless sintering in air and inert atmospheres. (iii) A description of various applications of SiC ceramics; (iv) a discussion of current limitations and strategies for improving the performance of SiC ceramics.

2. AM technologies for SiC ceramics

SiC AM is less advanced compared to oxide ceramics, primarily because of several challenges, including limited material flexibility, sintering and performance issues. Indeed, all AM technologies (based on slurries, powders, filaments, and sheets) have been adapted to process SiC-based structures, each presenting unique challenges and advantages, requiring specific optimization to achieve desired material properties and structural integrity[8,9].

The selection of an appropriate additive manufacturing technique and post-processing strategy for SiC-based ceramic components depends on specific application requirements. Major AM techniques, categorized by printing precision and process characteristics, as shown in Table 1, include: ultra-high precision (two-photon polymerization, TPP), high precision (stereolithography, SL; digital light processing, DLP; and inkjet printing, IJP), moderate precision (selective laser sintering, SLS; selective laser melting, SLM; and binder setting, BJT), low precision (direct ink writing, DIW; and fused deposition modeling, FDM), and ultra-low precision for bulk structures (laminated object manufacturing, LOM)[8]. Here, TPP, SL, and DLP techniques belong to the Vat photopolymerization process; IJP, DIW, and FDM belong to the material extrusion process; BJT belongs to the material jetting process; and SLS and SLM belong to the laser−powder bed fusion process. From the material processing perspective, SiC-based ceramics can be fabricated either indirectly (e.g., through precursor

Table 1. Overview of additive manufacturing technologies used in the fabrication of ceramics.

Technologies	Printing accuracy	Accuracy range	Type of feedstock	Efficiency
TPP	Ultra-high	50–200 nm	Slurry	Ultra-low
SL/DLP	High	500 nm–100 μm		Low
IJP	Moderate	50 μm–200 μm		Moderate
SLS/SLM		100 μm–300 μm	Powder	
BJT		100 μm–300 μm		
FDM	Low	200 μm–2 mm	Filament	High
DIW		200 μm–3 mm		
LOM	Ultra-low	500 μm–10 mm	Bulk	Ultra-high

conversion or preform reaction sintering) or directly using solid SiC-based feedstocks[4]. This review describes recent research advances in the additive manufacturing of SiC ceramics and their applications; both qualitative and quantitative analyses are presented to evaluate the performance and potential of these technologies.

2.1. Research progress in ultra-high precision additive manufacturing of SiC/SiOC-based ceramics (two-photon polymerization, TPP)

Among the various additive manufacturing technologies, two-photon polymerization (TPP) represents the most precise approach with nanoscale resolution. Two-photon absorption (TPA) was first proposed by Maria Goeppert Mayer in her 1931 doctoral dissertation and later experimentally confirmed in 1961 by Kaiser and Garrett during the excitation of a CaF_2: Eu (II) crystal through the absorption of red light followed by blue fluorescence[10]. Based on photopolymerization principles (Figure 2(a)), TPP is excited via simultaneous absorption of two photons from a near-infrared (∼780 nm) or green (∼515 nm) laser, inducing cross-linking within a tightly focused spot in the photosensitive resin for polymerization. By programming the laser path, three-dimensional structures are fabricated[11]. A key advantage of TPP as a micro/nanofabrication tool is its ability to polymerize sub-focal volumes within liquid polymer resins, achieving high-precision shaping (∼100 nm). This relies on the focused light to induce curing, and TPP typically requires transparent resin systems. In the microfabrication of ceramics, it has been primarily used with preceramic polymers (PCP) and sol-gel precursors.

The first study on the fabrication of 3D SiC/SiOC-based polymer-derived ceramics with sub-micrometer resolution via TPP was conducted by Pham et al. in 2006, who employed a newly developed photosensitive inorganic PCP with a high ceramic yield[15]. In a later report in 2018[16], acrylate-modified silicon sources were used in TPP to fabricate lattice structures with a printing resolution of about 350 nm, and they also fabricated large-scale architectures. After pyrolysis, SiOC ceramic structures were obtained, albeit with over 50% volumetric shrinkage. Subsequently, Lorenzo's group[13] used a thiol-functionalized silicon resin system in TPP, reducing the shrinkage after pyrolysis to around 30% (Figure 2(b)), with the compressive strength of the micro-nano structures reaching 7 GPa (Figure 2(c)). Similarly, another work used a carbon-rich polysiloxane (SPR-684) in TPP, achieving preceramic structures with ∼350 nm resolution. After pyrolysis, the shrinkage perpendicular to the printing direction was controlled to within 30% (Figures 2(d) and (e))[14].

To date, direct fabrication of micro/nano SiC components via TPP remains in early-stage research, primarily because of the inferior stability and forming accuracy of SiC precursors compared with those of other silicon-based systems, with limited substantial results. Current research on TPP-fabricated polymer-derived ceramics focuses on material development, post-processing, and micro-mechanical characterization. Moving toward practical applications requires addressing two major challenges: shrinkage remains inadequately controlled at around 30%, often causing structural deformation, and limited research focused on real-world applications of these micro/nanoceramics, offering little reference for their implementation at larger scales.

2.2. Research progress in high-precision additive manufacturing of SiC (stereolithography (SL)/digital light processing (DLP))

Similar to two-photon polymerization (TPP), SL and DLP, these methods utilize photopolymerization, offering high manufacturing accuracy. Among these, the SL process (Figure 3(a)) uses an ultraviolet laser to selectively scan and crosslink the resin within the slurry, solidifying each layer point-by-point. The structure is built layer-by-layer through repeated recoating and exposure, forming 3D objects in a point-line-surface sequence. This scanning-based method offers high precision due to minimal heat accumulation, though it has a relatively slow fabrication speed[17].

Different from SL technology, DLP utilizes light exposure instead of point scanning. Depending on the relative position of the build platform and the projection unit, DLP can be classified into "bottom-up" (Figure 3(b)) and "top-down" printing modes (Figure 3(c)). Compared with the "bottom-up" configuration, the "top-down" mode allows for larger build sizes and greater compatibility with a wider range of slurry systems.

Analogously, SL/DLP additive manufacturing of SiC green bodies can be categorized into three main approaches: direct printing of solid SiC materials, curing of preceramic polymers, and reaction sintering of cured preforms to produce SiC-based ceramic structures[4].

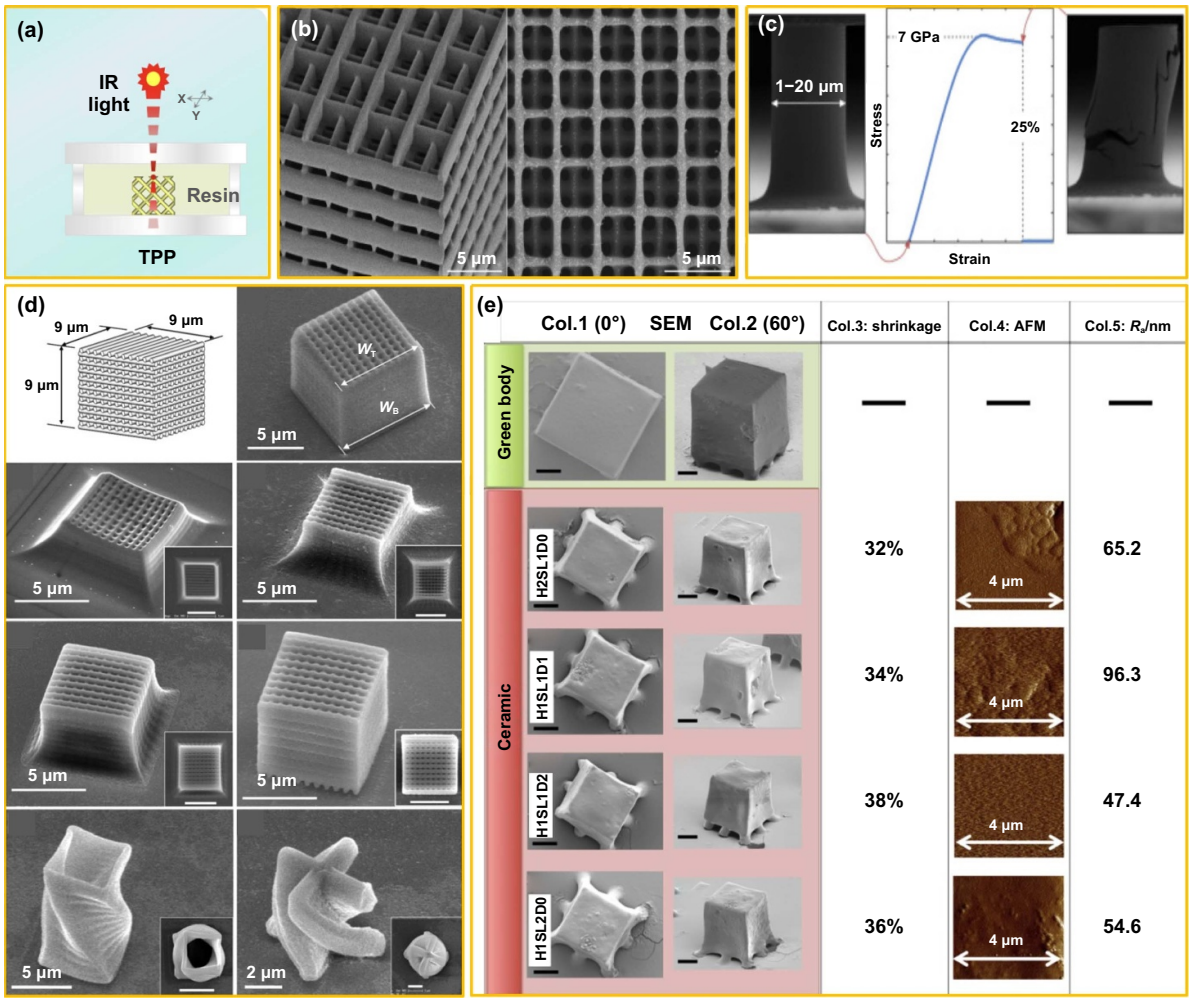


Figure 2. Research on SiC/SiOC-based ceramics fabricated by TPP. (a) Schematic diagram of the SL process. Reprinted from[12], Copyright (2022), with permission from Elsevier. (b) As-printed polymeric and pyrolyzed SiOC octet nanolattice. (c) SEM images of pillars before testing and at failure, along with stress−strain curves. (b), (c) Reprinted from[13], Copyright (2019), with permission from Elsevier. (d) SEM and AFM images (Col. 1, 2, and 4) of ceramic cubes printed with different parameters, with corresponding mean values of linear shrinkage (Col. 3) and average roughness (scale bar: 10 μm). (e) Three-dimensional ceramic microstructures fabricated by nano-SL and subsequent pyrolysis at 600 °C. (d), (e) Reprinted from[14], Copyright (2020), with permission from Elsevier.

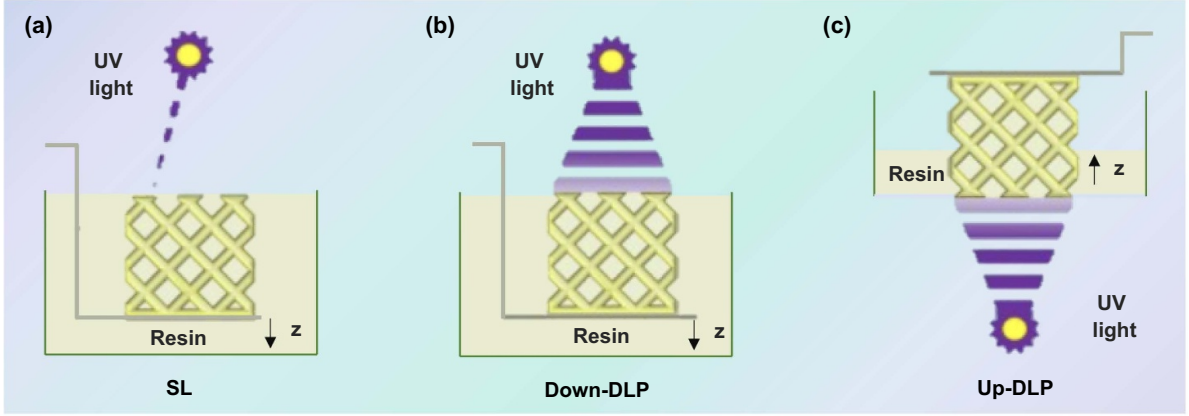


Figure 3. Schematic diagram of the SL/DLP process. (a) Schematic diagram of the SL process. (b) Schematic diagram of the down-DLP process. (c) Schematic diagram of the Up-DLP process. Reprinted from[12], Copyright (2022), with permission from Elsevier.

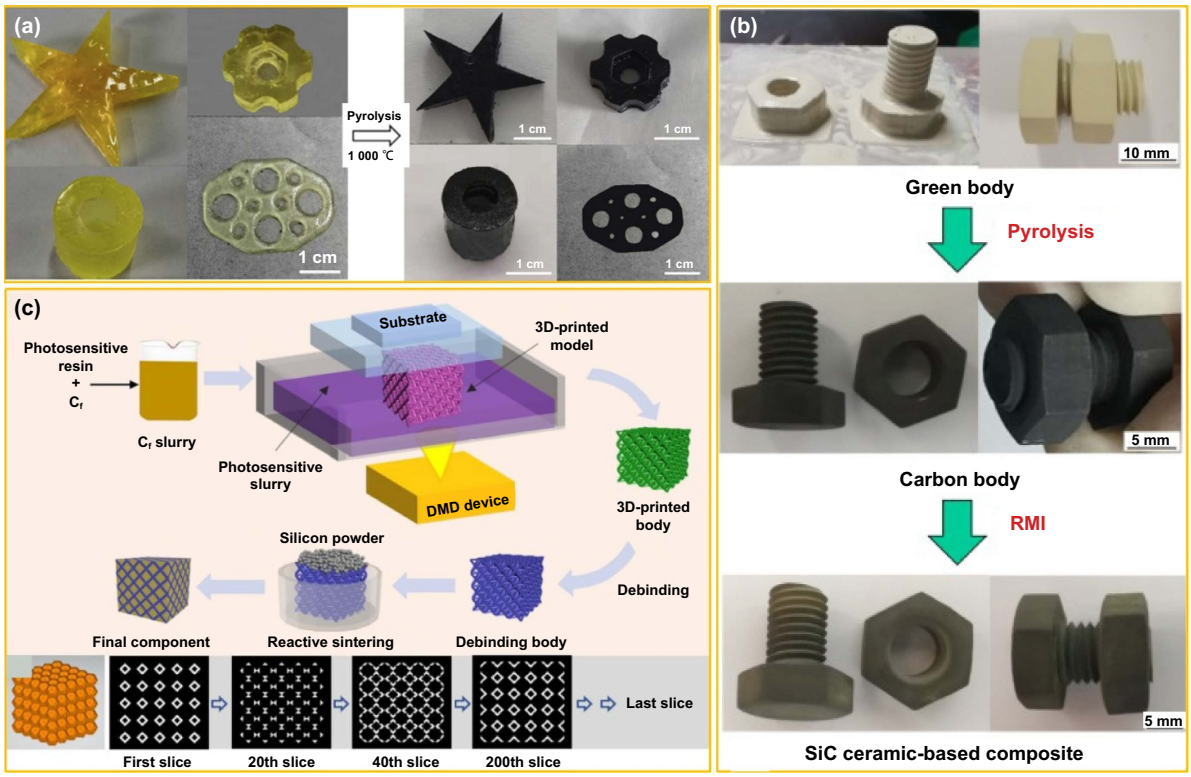


Figure 4. Fabrication of SiC ceramics by SL/DLP without SiC-based material. (a) SiC manufactured via DLP 3D printing and ceramic precursor pyrolysis. Reprinted from[21], Copyright (2017), with permission from Elsevier. Reprinted from[22], Copyright (2020), with permission from Elsevier. (b) SiC-based ceramics by DLP-fabricated C preforms and liquid-phase silicon infiltration reaction sintering. Reprinted from[23], Copyright (2021), with permission from Elsevier. (c) SiC-based structural ceramics via DLP shaping of Cf/C preforms with liquid-phase silicon infiltration reaction sintering. Reprinted from[24], Copyright (2020), with permission from Elsevier.

2.2.1. Fabrication of SiC/SiOC ceramics by SL/DLP without SiC-based materials. Owing to the high ultraviolet absorption and scattering coefficients of SiC particles, research on fabricating SiC-based ceramics via precursor conversion or preform reaction sintering emerged relatively early. In 2015, Colombo et al. reported for the first time on the additive manufacturing of SiOC ceramic micro-components using an engineered photosensitive methyl-silsesquioxane preceramic polymer[18]. Eckel et al.[19] employed DLP to fabricate ceramic precursors, producing SiOC ceramics at a relatively low temperature of 1 000 °C. However, precise control of the elemental composition remains challenging, preventing complete conversion to phase-pure SiC ceramics. de Hazan and Penner[20] subsequently produced SiC/SiOC composite ceramics using a modified silicon-based precursor. As shown in Figure 4(a), a hyperbranched polycarbosilane (LHBPCS) precursor was developed[21,22]. By optimizing the precursor composition, near-stoichiometric control of Si and C was achieved, resulting in SiC ceramics with an atomic ratio close to 1:1. Chen et al.[23] employed a combined DLP and RMI technique, first printing and sintering diamond material to form a carbon structure and then utilizing a reactive melt immersion (RMI) sintering process to control the formation of the silicon carbide matrix phase, thereby producing SiC-based components. This approach circumvented the challenges of direct photopolymerization of SiC powders, achieving a flexural strength of 460 MPa in the resulting SiC ceramics (Figure 4(b)). Similarly, C/Cf preforms were prepared via vat photopolymerization and subsequently transformed into SiC-based ceramics through RMI, endowing the printed parts with a mechanical strength of 262.6 MPa[24]. However, the indirect VPP of SiC-based ceramics results in high linear shrinkage (>20%) in the manufacturing process of C preforms, making it difficult to ensure the dimensional accuracy of the final SiC ceramic parts (Figure 4(c)). Owing to its limited precision and dimensional control, this indirect forming approach shows little promise for practical application validation.

2.2.2. Fabrication of SiC ceramics by SL/DLP from SiC feedstock. Compared to indirect fabrication, direct fabrication of SiC structures via SL/DLP using solid materials offers advantages in shrinkage control and dimensional accuracy and has thus attracted broader research interest. However, the high ultraviolet absorption of SiC powder poses significant challenges for direct processing. To improve the photocuring performance of SiC slurries, researchers have pursued three main strategies:

First, optimization of the resin or inorganic matrix. Pioneering studies on the effects of dispersants and resins were performed by Ding et al.[25], who fabricated SiC parts

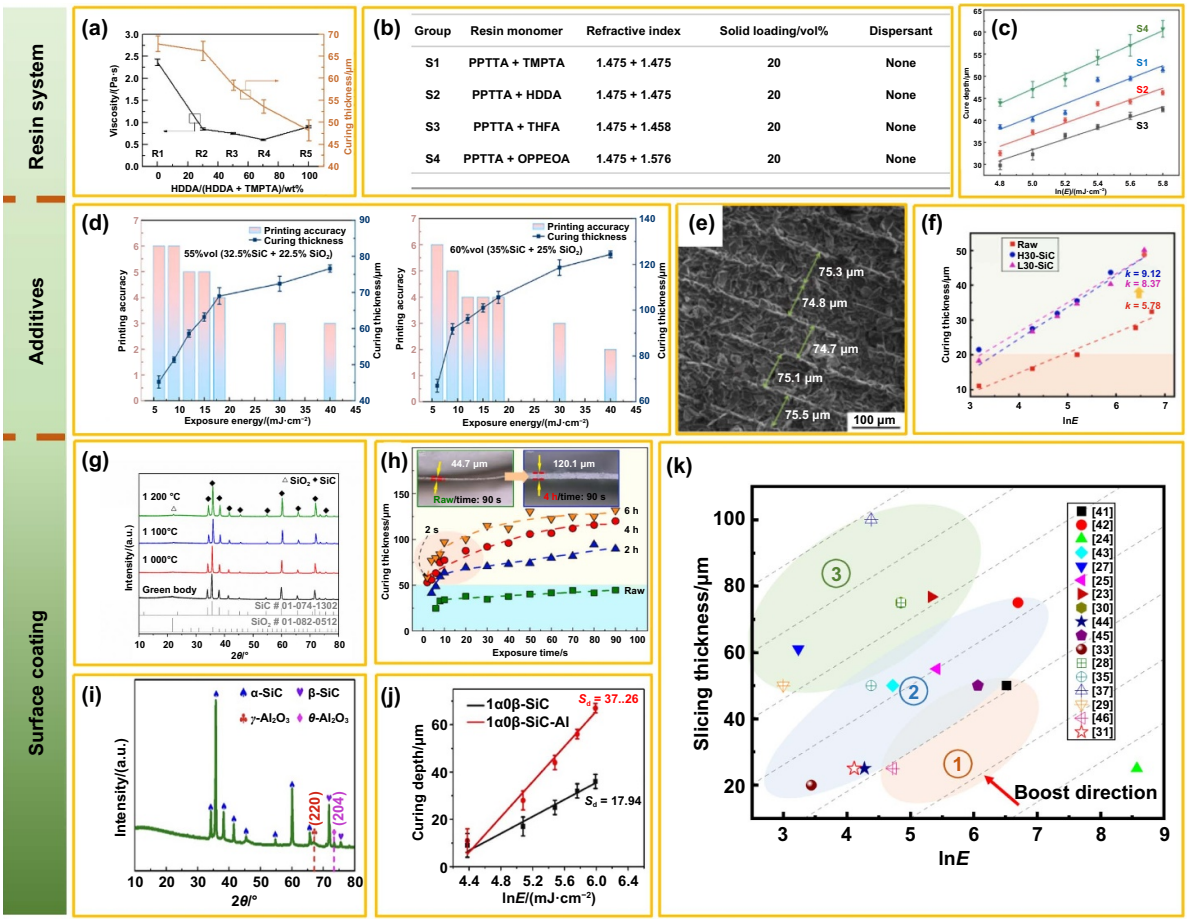


Figure 5. SL/DLP direct fabrication of SiC-based structural ceramics. (a) Tuned resin ratio to improve the printability of the slurry. Reprinted from[25], Copyright (2020), with permission from Elsevier. (b), (c) Comparison of the curing properties of slurries composed of resins with different refractive indices. Reprinted from[26], Copyright (2022), with permission from Elsevier. (d) Printing accuracy versus different energy exposures improved the curing performance of the SiC slurry. (e) SEM image of the curing depth of the fabricated layer. (d), (e) Reprinted from[27], Copyright (2023), with permission from Elsevier. Reprinted from[28], Copyright (2022), with permission from Elsevier. (f) Comparison between hydrophilic and oleophilic SiO_2 additions in improving the curing depth of the SiC slurry. Reprinted from[29], Copyright (2024), with permission from Elsevier. (g) XRD analysis of the SiC powders with different pre-oxidation times. (h) Pre-oxidation of SiC powder to increase the curing thickness of the slurry. Reprinted from[30], Copyright (2021), with permission from Elsevier. (i) XRD image of Al_2O_3-coated SiC powder. (j) Effect of coating modification on the curing depth and over-curing width. (i), (j) Reprinted from[31], Copyright (2024), with permission from Elsevier. (k) Comparison of curing performances from the literature[23–25,27–29,32–42].

with improved curing performance (Figure 5(a)). Inspired by AM-Si_3N_4, Zou et al.[26] reduced the refractive index mismatch between the resin and powder, improving the curing depth of the slurry by nearly 50% (Figures 5(b) and (c)).

Second, incorporation of low-absorption powders—such as Al_2O_3[32] or SiO_2[27,28,33]—to improve printability. Yang et al.[27,28] examined the effects of adding 30 vol% SiO_2 to formulate a 60 vol% solid-loaded SiC/SiO_2 slurry with a curing depth exceeding 120 μm, achieving a 75 μm layer thickness for rapid prototyping. Using a two-step process of reaction sintering (converting SiO_2 to SiC whiskers) followed by reactive melt infiltration (RMI), high-purity SiC ceramics were produced with a flexural strength of (268.66 ± 10.19) MPa (Figures 5(d) and (e)). Furthermore, hydrophilic and hydrophobic SiO_2 additives were compared, and it was found that the inclusion of 30 vol% SiO_2 (relative to the total powder content) doubled the curing performance, as shown in Figure 5(f)[29,43].

Third, coating SiC particles with inorganic layers to reduce light absorption, using methods such as pre-oxidation[30,34–36,44] or sintering of inorganic coatings[31,45,46]. Chen et al.[30,34] pioneered a pre-oxidation method to fabricate core-shell SiC@SiO_2 particles at 1 200 °C for 4 h (Figure 5(g)), improving the curing depth threefold compared to that of untreated SiC powder (Figure 5(h)). Combined with precursor pyrolysis sintering, SiC@SiO_2/SiOC ceramics were manufactured with a compressive strength of 37 MPa. Subsequently, the combination of pre-oxidation and reactive melt infiltration (RMI) was employed to fabricate SiC ceramics, achieving a density of 2.87 g·cm^{-3} and a flexural strength of 267.52 MPa[36]. In a similar approach utilizing pre-oxidation, the strategy of particle size gradation enabled the manufacture of pressureless-sintered SiC composites with a flexural strength of 170.9 MPa[35,44]. To further enhance the process, an AlOOH solution was mixed with SiC powder via magnetic stirring and subsequently calcined,

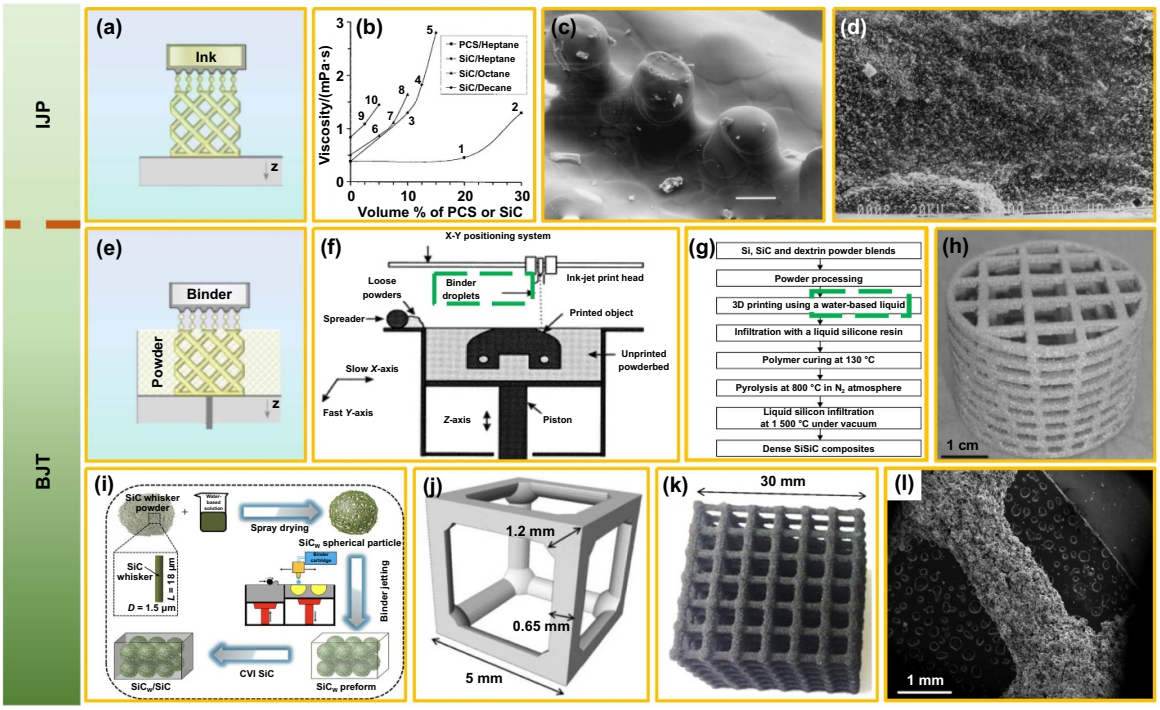


Figure 6. Fabrication of SiC-based structural ceramics based on IJP or BJT. (a) Schematic of the IJP process. Reprinted from[12], Copyright (2022), with permission from Elsevier. (b) Ink viscosity versus polycarbosilane or silicon carbide concentration in different solvents. (c) Top surface of the components printed with polycarbosilane ink. (d) Fracture face of the printed blocks after pyrolysis. (b)–(d) [48] John Wiley & Sons. © The American Ceramic Society. (e) Schematic of the BJT process. Reprinted from[12], Copyright (2022), with permission from Elsevier. (f) BJT process based on liquid adhesive moulding. Reprinted from[50], Copyright (2001), with permission from Elsevier. (g), (h) BJT process based on solid adhesive moulding and the resulting part. Reprinted from[51], Copyright (2013), with permission from Elsevier. (i) Schematic of the fabrication procedure for SiC_W/SiC. Reprinted from[52], Copyright (2019), with permission from Elsevier. (j) Designed STL cubic unit cell. (k) Printed cellular lattice structure. (l) SEM image of the structure. (j)–(l) Reprinted from[53], Copyright (2020), with permission from Elsevier.

producing a $SiC@Al_2O_3$ core-shell powder[31,46] (Figure 5(i)). This coating method not only more than doubled the curing depth (Figure 5(j)) to facilitate photopolymerization but also contributed to a final composite flexural strength of 225.3 MPa. These studies collectively demonstrate that targeted pre-treatment and microstructural design strategies are effective in significantly enhancing the manufacturability and mechanical properties of SiC-based ceramics.

The SiC-based slurries prepared in the literature are compared in Figure 5(k)[29]. All the studies can be divided into three categories: Group ① includes studies focused on pure SiC slurries, Group ② includes those with low solids content ($\leq$35%) or large particle sizes (D50 $>$ 15 μm), and Group ③ includes studies with larger SiC particles (D50 $>$ 15 μm) and additives. Among the various methods, the pre-oxidation of SiC significantly enhances the curing depth, offering an efficient and facile approach and making it a promising route for fabricating SiC structural ceramics.

2.3. Research progress in moderate-precision additive manufacturing of SiC

2.3.1. Inkjet printing (IJP). Inkjet printing (IJP) is an extrusion-based deposition technique in which liquid inks are ejected from printed nozzles onto substrates to create precise 2D patterns and structures (Figure 6(a)). Three-dimensional structures are formed through the layer-by-layer stacking of these patterns[47]. In 2001, Mott and Evans[48] formulated inkjet inks by mixing precursors with SiC particles and characterized their rheological behavior. Figure 6(b) shows that the addition of small amounts of SiC particles significantly increased the ink viscosity. While structures printed with only precursor materials exhibited good surface quality (Figure 6(c)), such structures remained prone to sintering defects such as cracking during pyrolysis. In contrast, inks with SiC particles provided improved microstructural integrity after pyrolysis (Figure 6(d)). Notably, IJP shows promise for fabricating thin-layer structures with fine ceramic particles, offering advantages such as being economical and easy to print, but its limited vertical printing height ($<$1 mm)[49] makes this technology better suited for the manufacturing of functional thin-layer devices rather than high-height structural components.

2.3.2. Binder jetting (BJT). Binder Jetting (BJT) is similar to the inkjet printing of ceramics; however, in this case, the ceramic material is not ejected by the nozzles but by a binder. As shown in Figure 6(e), the process involves selectively depositing a liquid onto a powder bed to bond particles

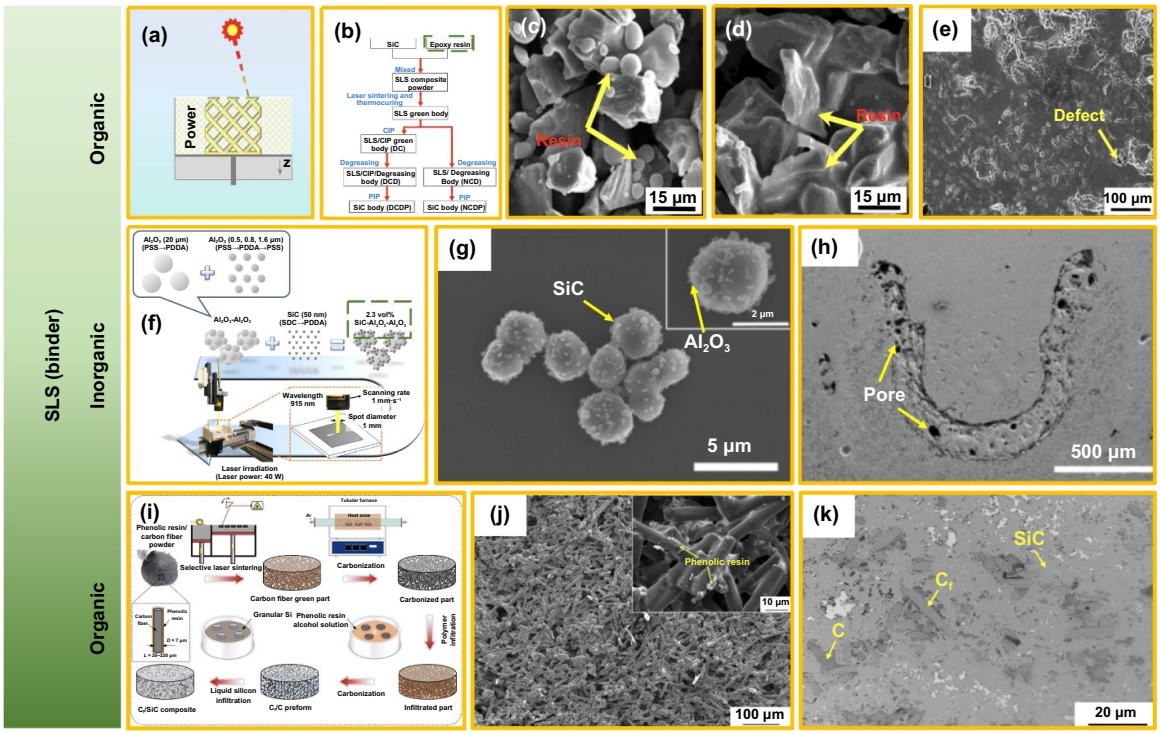


Figure 7. Fabrication of SiC-based structural ceramics based on SLS or SLM. (a) Schematic diagram of the SLS process. Reprinted from[12], Copyright (2022), with permission from Elsevier. (b) Fabrication process for SiC composites using SLS with organic binders. (c) SEM image of a specimen after laser sintering. (d) SEM image of a specimen after thermal curing. (e) SEM image of a specimen after PIP. (b)–(e) Reprinted from[56], Copyright (2018), with permission from Elsevier. (f) Fabrication process for the SiC/SiC components using SLS based on inorganic binders. (g) Morphologies of the electrostatic nano-assembled SiC–Al_2O_3 composite particles. (h) Cross-sectional morphology images of the laser-irradiated SiC–Al_2O_3 composite particles. (f)–(h) Reprinted from[57], Copyright (2021), with permission from Elsevier. (i) Schematic illustration of the procedure for fabricating C_f/SiC composite parts. (j) SEM image of the SLS green part. (k) SEM image of the cross section of Cf/SiC after LSI. (i)–(k) Reprinted from[58], Copyright (2018), with permission from Elsevier.

layer-by-layer, gradually building a three-dimensional object. The binder (organic or inorganic) can either be jetted directly from the nozzles[50,52,54] or be introduced in the powder bed in the form of powders that react or dissolve in contact with a reactive or inert liquid jetted from the nozzles[51,55].

In 2001, a team at MIT[50] employed a furan resin and furfuryl alcohol binder to fabricate SiC green bodies via BJT, followed by reactive melt infiltration to produce complex Si/SiC ceramics with overhangs, undercuts, and internal channels (Figure 6(f)), demonstrating the feasibility of the process. Alternatively, the addition and dissolution of solid dextrin powder in a SiC powder bed by water jets from the nozzles was used to form SiC green bodies[51] (Figure 6(g)), which were consolidated by liquid silicon infiltration to fabricate Si/SiC ceramics (Figure 6(h)).

The BJT process exhibits good adaptability to various raw materials, including whiskers and fibers. For example, Lv et al.[52] combined binder jetting with chemical vapor infiltration (CVI) to fabricate SiC whisker-reinforced SiC composites that reached a flexural strength of 200 MPa (Figure 6(i)). However, in terms of dimensional accuracy, the work by Baux et al.[53] reported that BJT-printed SiC ceramics exhibit significant deviations from the original model (Figure 6(j)), particularly in lattice structures where surface flatness is relatively poor (Figures 6(k) and (l)). However, despite its advantages in printing speed and suitability for large-format and sizable components, BJT faces limitations in dimensional control and residual porosity, often resulting in low shape accuracy and high surface roughness.

2.3.3. Selective laser sintering/melting (SLS/SLM). Like BJT, selective laser sintering (SLS) uses a high-power laser beam to selectively sinter powder particles layer-by-layer, enabling large-area bonding. This process is repeated layer by layer until a 3D part is fully formed (Figure 7(a)). Significantly, SLS 3D printing is widely adopted for processing ceramic materials, driving increasing research on its application to SiC ceramics.

Owing to the high sintering temperature of SiC, its processing via SLS 3D printing typically requires the mixing or coating of sintering aids. Based on material composition, these techniques can be classified into two categories: those using organic and those using inorganic additive binders. Organic binders such as phenolic resin[58–61], epoxy resin[56,62], and other materials[63,64] have been widely used. SLS was utilized to fabricate components from epoxy resin mixed with SiC powder, producing ceramics with a flexural strength of 201 MPa and an elastic modulus of 1.27 GPa[56] (Figures 7(b)–(d)). Although more complex to prepare, inorganic additives

can yield green parts with higher mechanical strength. By employing SLS with a mixture of PMS and SiC powder, green bodies with a flexural strength of 17 MPa significantly greater than that of polymer-based systems, were achieved[64]. Alternatively, Al_2O_3–SiC powders suitable for direct SLS processing were prepared using an electrostatic nano-assembly technique[57] (Figures 7(f)–(h)).

Although inorganic binders offer better mechanical properties in green parts fabrication, their complex and time-consuming powder preparation makes organic binders more prevalent. SLS also exhibits good material adaptability. For instance, Shi et al.[58] fabricated parts from a phenolic resin-coated carbon fiber powder using SLS 3D printing, and after liquid silicon infiltration, the flexural strength reached 249 MPa (Figures 7(i)–(k)). This demonstrates that SLS-formed SiC green bodies can be indirectly processed into dense ceramics.

Selective laser melting (SLM), a derivative of SLS uses higher laser energy to fully melt the powder bed, resulting in denser and more homogeneous structures. However, SLM is less suitable for high-melting-point SiC powders, where rapid heating and cooling characteristics often lead to cracks[65]. SLM is more commonly used for metal matrix composites reinforced with SiC. For example, Wei et al.[66] successfully fabricated SiC-316L composites by incorporating SiC ceramic particles into 316L stainless steel. Microstructural analysis shows that the SiC particles remain largely unaffected by the laser melting—instead, they are bonded by the molten stainless steel, enabling the formation of SiC-based composites.

Similar to BJT, both SLS and SLM face challenges in dimensional accuracy and surface finish due to powder splatter and melt pool instability. However, these techniques remain well-suited for producing large-format and sizable components.

2.4. Research progress in low-precision additive manufacturing of SiC

2.4.1. Direct ink writing (DIW). Direct ink writing (DIW) was first developed in 1996 at Sandia National Lab.oratories in the USA, using an extrusion-based process, and it was labeled "Robocasting". The technique extrudes ink through a nozzle via mechanical or pneumatic means to form continuous filaments, which are deposited layer by layer to build three-dimensional objects (Figure 8(a))[67].

Printing quality depends greatly on slurry properties, printing parameters, and curing thickness. Because of the unique extrusion mechanism, DIW offers broad adaptability to various slurry compositions and enables the fabrication of large-sized components. DIW of SiC-based ceramics can be categorized into three types: liquid-based SiC precursor printing[68,69], liquid precursors mixed with solid SiC particles[70,71,76–78], and solid-phase SiC printing[72,73,79]. In liquid precursor-based DIW, Larson et al.[68] employed SiC colloid and boron-modified polycarbosilane (BPCS) to fabricate microwave optical devices with good structural integrity (Figures 8(b)–(d)). Similarly, Chen et al.[69] used xylene-dissolved polycarbosilane as a precursor ink to form SiC structures, which were subsequently pyrolyzed to produce ceramics. The same team later investigated SiC whisker-reinforced precursors[70,71], achieving a tensile strength of 47.3 MPa in the final SiC composites after chemical vapor infiltration (Figures 8(e)–(h)). However, liquid precursor-derived SiC structures often exhibit low strength and poor compatibility with densification processes, making them of limited technological interest.

In contrast, DIW using SiC powders or mixtures of liquid precursors with solid SiC particles has gained increasing attention. For instance, Lu et al.[72,73] incorporated short fibers into SiC-based slurries and studied the effects of the nozzle diameter and printing parameters on fiber alignment, concluding that smaller nozzles promote more ordered fiber orientation. Using precursor infiltration and pyrolysis, they manufactured SiC samples with a flexural strength of 274 MPa (Figures 8(i) and (j)). Solid-phase SiC slurries are particularly advantageous due to their high solid loading, low degree of sintering shrinkage and low organic content, which has driven increased research focus on solid-phase-based DIW for SiC ceramics.

2.4.2. Fused deposition modeling (FDM). FDM, also known as fused filament fabrication (FFF), is a material extrusion-based AM process. During processing, a polymeric filament is continuously fed into a moving nozzle, where it is heated above its melting point and extruded in a liquid state. The extruded material is deposited layer by layer according to a predefined path to construct three-dimensional structures (Figure 8(k)). Commonly used thermoplastic filaments include polylactic acid (PLA), polyether ether ketone (PEEK), and their composites[80–83]. Recent advancements in FDM technology have expanded its use to fabricate metallic[84,85] and ceramic materials[74,82,86,87]. Zhang et al.[74,87] used SiC-precursor filaments in FDM to manufacture green bodies, which were pyrolyzed to obtain high-purity SiC ceramics (Figure 8(l)). Among the various thermoplastic blends studied, the highest ceramic content (50%) was achieved with a rubber precursor, and the lowest volumetric shrinkage (30%) resulted from flexible PLA mixtures. Additionally, the integration of shape memory effects into SiC/C/PLA composite structures has been accomplished through FDM[82]. The successful densification of wire-printed SiC components was also realized via pressureless sintering, employing a high heating rate of 10 $^{\circ}C\cdot min^{-1}$ and utilizing carbon derived from the binder[88]. These studies collectively demonstrate that by flexibly adjusting the precursor composition and processing pathways via FDM, it is possible to effectively regulate the composition, structure, and functional properties of SiC-based ceramics while enabling the formation of complex shapes.

However, conventional FDM of SiC ceramics provides limited mechanical advantages compared to direct ink writing, mainly due to lower solid loading in the filaments. Consequently, recent research has shifted toward the development of continuous-fiber-reinforced SiC

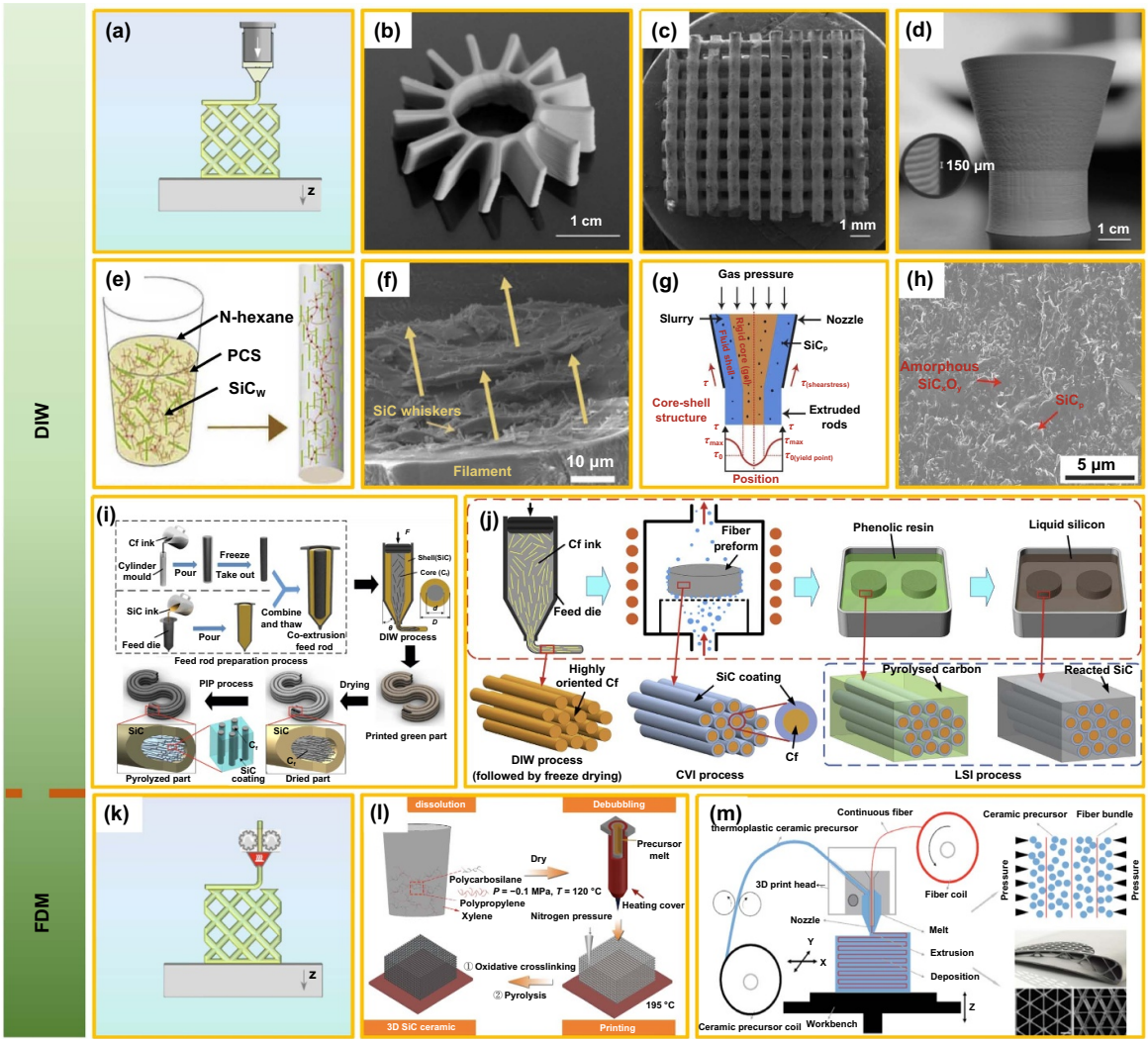


Figure 8. Fabrication of SiC-based structural ceramics based on DIW or FDM. (a) Schematic of the DIW process. Reprinted from[12], Copyright (2022), with permission from Elsevier. (b) As-printed turbine fan. (c) Sintered periodic lattice. (d) As-printed microwave feedhorn with ≈150 μm wall thickness. (b)–(d) [68] John Wiley & Sons. © 2015 WILEY-VCH Verlag GmbH & Co. KGaA, Weinheim. (e) Composite DIW ink. (f) Aligned SiC whiskers inside the filament. (g) Extrusion process of a core−shell rod. (h) Morphology of samples heat treated at 1 000 °C in Ar for 2 h[69–71]. (e)–(h) Reprinted from[69], Copyright (2018), with permission from Elsevier. Reprinted from[70], Copyright (2020), with permission from Elsevier. Reprinted from[71], Copyright (2019), with permission from Elsevier. (i) Schematic of the preparation of C_f/SiC core/shell parts. Reprinted from[72], Copyright (2019), with permission from Elsevier. (j) Schematic of the preparation of carbon fiber-reinforced SiC ceramic composite (Cf/SiC) partsReprinted from[73], Copyright (2019), with permission from Elsevier. (k) Schematic of the FDM process. Reprinted from[12], Copyright (2022), with permission from Elsevier. (l) Schematic of SiC 3D structure fabrication. Reprinted from[74], Copyright (2021), with permission from Elsevier. (m) Schematic of continuous-fiber 3D printing of SiC ceramics. [75] John Wiley & Sons. © 2018 The American Ceramic Society.

composites via FDM[75,89,90]. For instance, Mei et al.[75] fabricated continuous-fiber-reinforced SiC ceramics using FDM, pyrolysis, and chemical vapor deposition, achieving a flexural strength of 120.2 MPa (Figure 8(m)). Similarly, Li et al.[89,90] employed FDM, followed by precursor infiltration and pyrolysis (PIP), to fabricate SiC-based ceramics with a flexural strength of 149.1 MPa and further used chemical vapor infiltration (CVI) to impart wave-absorbing properties. Collectively, these studies on continuous fiber reinforcement represent a significant developmental direction, shifting from traditional low-solid-loading printing toward the fabrication of high-performance, multifunctional composite materials.

2.5. Ultra-low precision additive manufacturing of SiC (laminated object manufacturing (LOM))

The Dimatteo patent marked the beginning of LOM printing technology, which was first proposed in 1974[91]. LOM creates 3D parts by bonding adhesive-coated sheets layer by layer. Adhesion between layers is typically achieved through simultaneous heating and mechanical compression (Figure 9(a)). LOM was first applied to ceramic additive manufacturing in 1994. In 2004, Greil et al. used this technique to fabricate SiC-based ceramics (Figure 9(b)); microstructural analysis (Figure 9(c)) revealed significant interlayer

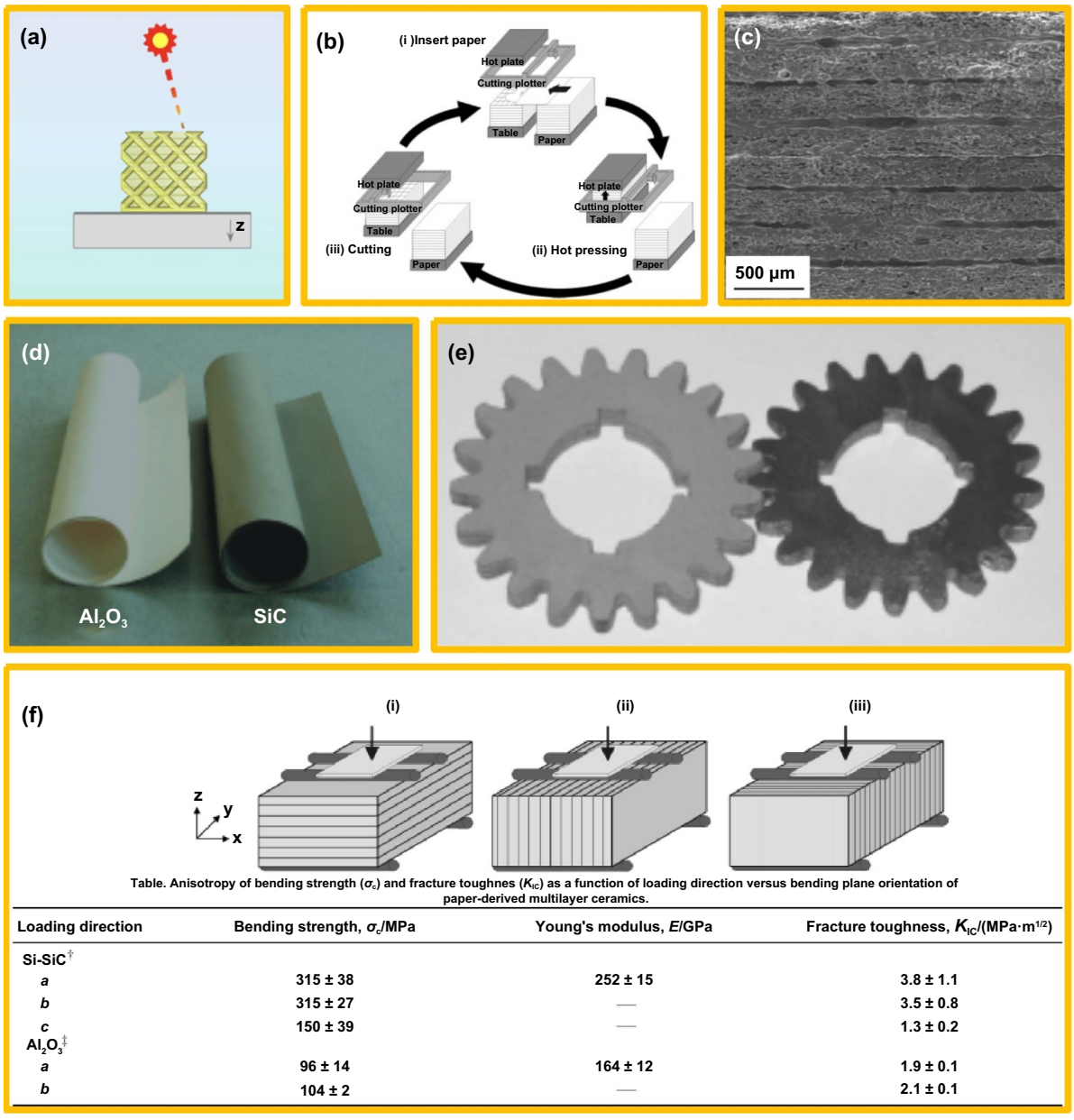


Table. Anisotropy of bending strength (σ_c) and fracture toughnes (K_{IC}) as a function of loading direction versus bending plane orientation of paper-derived multilayer ceramics.

Loading direction	Bending strength, σ_c/MPa	Young's modulus, *E*/GPa	Fracture toughness, K_{IC}/(MPa·m$^{1/2}$)
Si-SiC†			
a	315 ± 38	252 ± 15	3.8 ± 1.1
b	315 ± 27	—	3.5 ± 0.8
c	150 ± 39	—	1.3 ± 0.2
Al_2O_3‡			
a	96 ± 14	164 ± 12	1.9 ± 0.1
b	104 ± 2	—	2.1 ± 0.1

Figure 9. Fabrication of SiC-based structural ceramics based on LOM. (a) Schematic illustration of the LOM process. Reprinted from[12], Copyright (2022), with permission from Elsevier. (b) Schematic diagram of the fabrication process of SiC ceramics by LOM. (c) SEM image of the multilayer structure of a sample after infiltration with Si. (d) Schematic representation of a preceramic paper. (b)–(d) [92] John Wiley & Sons. Copyright © 2004 WILEY-VCH Verlag GmbH & Co. KGaA, Weinheim. [93] John Wiley & Sons. Copyright © 2007 WILEY-VCH Verlag GmbH & Co. KGaA, Weinheim. (e) Turbine rotor (diameter: 60 mm) manufactured from Al_2O_3-filler preceramic paper (left) and a gear wheel (diameter, 50 mm) fabricated from SiC-filled preceramic paper (right). (f) Bending strength anisotropy of the LOM-fabricated ceramic. (e), (f) [94] John Wiley & Sons. © 2008 The American Ceramic Society.

porosity. It has also been used in conjunction with liquid silicon infiltration to fabricate SiC parts with flexural strengths ranging from 150 to 315 MPa[92,93]. Additionally, LOM has enabled the production of gear components for mechanical testing, which revealed anisotropic properties in SiC ceramics due to interlayer porosity (Figures 9(d)–(f))[94]. Compared to other AM techniques, LOM faces significant challenges in raw material preparation, interlayer bonding, along with low dimensional accuracy for complex structures, which limits its advantages in terms of structural precision and performance.

3. Post-treatment processing of SiC-based green bodies

The post-processing of printed green bodies critically influences the dimensional control, strength, and performance of the final ceramic products[95]. Upon completion of the printing process, the resulting green body specimens require a series of processing steps to yield the final sample, with the post-processing procedures for printed SiC ceramic specimens being particularly lengthy. These post-processing procedures can be broadly categorized into four principal steps

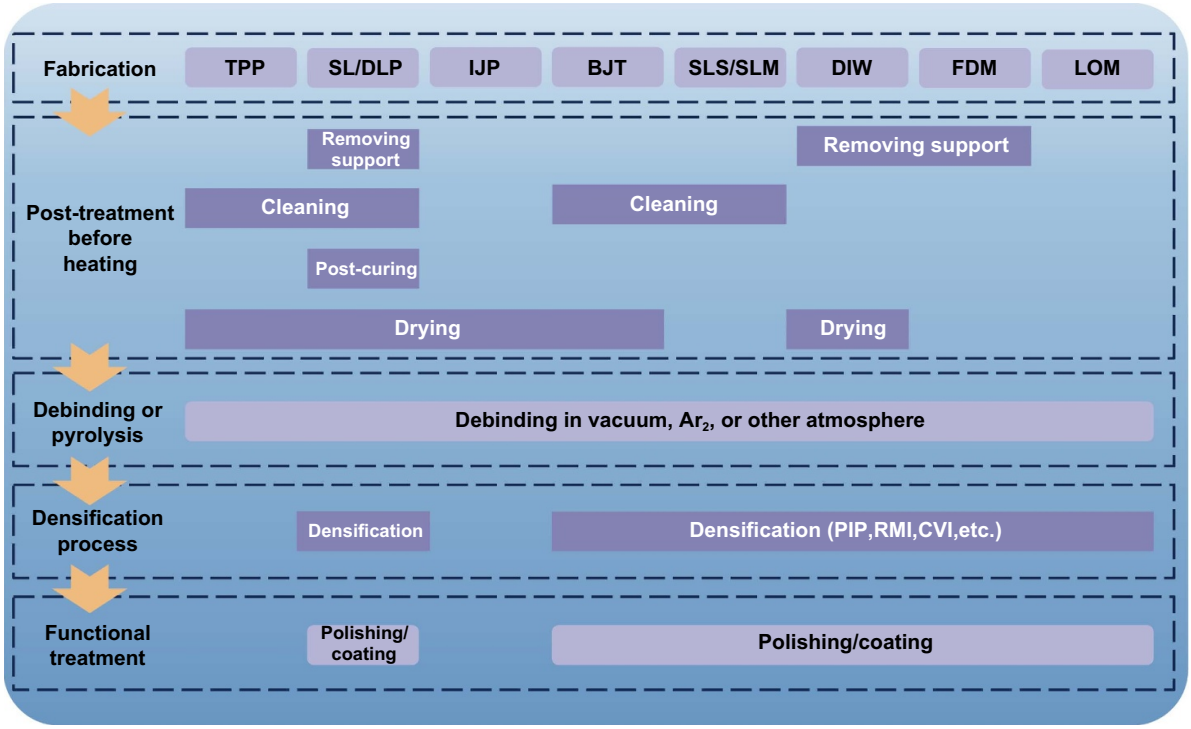


Figure 10. Post-treatment processes of SiC-based green bodies fabricated by the AM method.

(see Figure 10): the pre-heating treatment process, the debinding (also called degreasing) pyrolysis process, the densification (sintering) process, and functional post-treatment[55,96]. The following sections provide a detailed discussion of each of the aforementioned steps.

3.1. Post-treatments before heating

Before thermal treatments of a SiC-based green body, there are a series of processes employed to achieve high-quality and high-performance sintered SiC ceramics (Figure 10). When the printing procedure is finished, eventual support parts have to be removed from the fabricated green body. Depending on the manufacturing technique and feedstock, certain additive manufacturing processes can produce self-supporting structures, eliminating the need for dedicated support systems. Powder-bed methods such as IJP, BJT, and SLS/SLM inherently provide support via the surrounding powder. Likewise, two-photon polymerization (TPP) utilizes high-viscosity resins that enable self-supporting fabrication. In contrast, although inkjet printing (IJP) is generally not suited for tall or thick parts, this limitation similarly negates the requirement for support structures in practice. Subsequently, adhering to the obtained green body, the removal of excess material that does not contribute to the formed structure of the green body must be addressed[96]. During the cleaning process, there are generally two approaches: for printing methods based on slurry as the raw material, cleaning predominantly involves dissolution or liquid-based methods, whereas for processes utilizing powder particles as the manufacturing raw material, the focus is primarily on the simple mechanical removal of surface particles[97].

As for the post-curing step, this is primarily employed in SL/DLP processes[30]. Particularly in the fabrication of structural components, post-curing treatment is utilized to enhance the strength of the green body, thereby facilitating subsequent transfer and pyrolysis procedures. The final drying procedure corresponds to the previously mentioned cleaning step and is primarily aimed at removing excess cleaning fluid. The BJT process, however, is relatively unique in this regard, as it often employs a specific high-temperature drying stage[55,97,98]. This helps regulate the strength of the binder used during the forming process, ensures the structural integrity of the green body, and thereby prevents structural damage during subsequent handling and heat treatment. For TPP technology, drying primarily serves to remove the developer solution used during the cleaning process. With respect to the remaining additive manufacturing techniques, the necessity for a drying process is considerably less pronounced.

In summary, owing to variations in the form of raw materials, the processing of preforms before and after sintering differs across various additive manufacturing techniques. Consequently, various post-processing steps—including cleaning, drying, and curing—collectively serve as essential preparatory stages for the final heat treatment. Their primary function is to establish the necessary shape control and green strength as a prerequisite for successful sintering.

3.2. Debinding/pyrolysis

To remove water, binder, and organic materials from the green body, a debinding process (labelled pyrolysis when the decomposition of organic matter occurs in the absence of oxygen) is employed to transform the green SiC-body to

SiC-based ceramics. Generally speaking, the SiC parts possess high porosity and undergo high shrinkage after this process. According to the atmosphere, the debinding or pyrolysis processes can be divided into three groups: debinding in air, pyrolysis in vacuum, and pyrolysis in an inert gas atmosphere.

Debinding in air is a simple and cost-effective method compared to the other ones. It is not only easy to operate but also has no demanding requirements in equipment. However, sintering defects, including cracks and deformation, are prone to occur during debinding in air because of rapid mass loss of the green body and the occurrence of exothermic reactions. This issue is especially problematic for parts produced from low-solid-phase, high organic-content feedstocks through forming techniques such as IJP[99,100] and SL/DLP[101–103].

Pyrolysis in vacuum is a pre-sintering treatment step conducted in a continuously evacuated environment. By isolating the green body from atmospheric gases, it facilitates the pyrolysis of organic components, yielding a structure with residual carbon, which is a less disruptive process to the overall system with respect to combustion. These organic substances originate from the various additives employed in green body fabrication, including polymer precursors, binders, and resins. This vacuum-based technique has been applied to both oxide ceramics and non-oxide ceramics such as SiC[104,105] and Si_3N_4[106].

Pyrolysis in a controlled inert atmosphere helps prevent unintended reactions between ceramic particles and binders, thereby preserving the structural integrity of the ceramic[107]. The use of an inert atmosphere for debinding offers significant advantages in the rational design of ceramics, with Ar_2 and N_2 commonly employed as inert gases.

Debinding/pyrolysis of additively manufactured silicon carbide-based ceramics has been conducted in air, vacuum, and inert atmospheres. If precursor materials are used as the raw materials for additive manufacturing, the debinding process must be carried out in a vacuum or inert atmosphere to prevent oxidation of the silicon source[105]. Debinding of SiC-based ceramics in air is typically applied in processes involving pressureless liquid-phase sintering of SiC. For example, Shi et al.[44] fabricated SiC-based green bodies using vat photopolymerization. The parts were first pyrolyzed in an argon atmosphere furnace, followed by decarburization in air. Finally, the decarburized silicon carbide components were sintered in an atmosphere furnace. Debinding and sintering in nitrogen, argon, or vacuum have been investigated; however, no study has yet explicitly compared debinding and sintering processes for pure silicon carbide carried out in different atmospheres. With respect to SiC composite ceramics, Besisa et al.[108] compared the effects of debinding and sintering under argon/vacuum and nitrogen/vacuum atmospheres on the mechanical properties of SiC/AlN composites. The results showed that composites sintered in an Ar/vacuum atmosphere exhibited the best performance, characterized by a high density and homogeneous microstructure. It should be noted, however, that this study also included sintering steps. In terms of the debinding/pyrolysis stage alone, the influence of atmospheric variation is likely to be less pronounced.

3.3. Sintering and densification processes

After the debinding/pyrolysis process is completed, the production of dense SiC ceramics often requires specific processing steps. They include sintering and additional densification methods, which are used when the sintering process alone is not capable of producing a dense ceramic body. Currently, the primary methods employed for sintering and densification include direct pyrolysis, polymer infiltration and pyrolysis (PIP)[56,109], liquid phase sintering (LPS)[42,44], reactive melt infiltration (RMI)[61,110,111], chemical vapor infiltration (CVI)[53,112], and solid-state sintering (SSC)[113]. Among these methods, the SSC method typically demands raw SiC material with fine particle sizes (<2 μm), posing challenges in preparing feedstocks suitable for additive manufacturing[114,115]. Consequently, research in this area remains relatively limited.

For TPP technology, slurries struggle to use solid particle systems and typically require a densification post-processing step. Whilst IJP does involve printing with solid-particle inks, its SiC functional thin layers generally need to be compatible with the substrate. Such substrates often cannot withstand the high densification temperatures of SiC, rendering the densification process impractical.

The processes most suitable for the densification of additively manufactured SiC ceramics are illustrated in Figure 11. The one-step pyrolysis process primarily relies on SiC precursor materials, converting them into SiC ceramics through high-temperature cracking. Both the RMI and LSI densification principles involve the infiltration of molten silicon into the debound SiC ceramic green body, where it reacts with pyrolytic carbon to form additional SiC. Therefore, they are grouped together in this discussion.

Achieving high density in SiC-based ceramics is crucial to fully harness their structural integrity and functionality. Self-diffusion, a key mechanism in the sintering process, plays a significant role in achieving enhanced density and good mechanical properties. As shown in Figure 10, processes such as precursor pyrolysis, precursor infiltration and pyrolysis (PIP), liquid phase sintering (LPS), vapor phase infiltration, and reaction sintering result in varying density, phase purity, and dimensional shrinkage. On the other hand, processes such as PIP, reactive melt infiltration (RMI), and chemical vapor infiltration (CVI) offer better control over structural retention. Similarly, CVI, RMI, and PIP yield ceramics with superior purity and density. Moreover, as a high-performance material, SiC is challenging to sinter to high density and uniformity even when using these specialized densification methods. Contrarily, precursor pyrolysis (PP) and LPS offer significant advantages in terms of cost-effectiveness and processing efficiency, however, it should be noted that PP often results in amorphous ceramic materials.

3.4. Functional treatments

After undergoing debinding/pyrolysis and sintering/densification processes, SiC structural ceramics possess basic

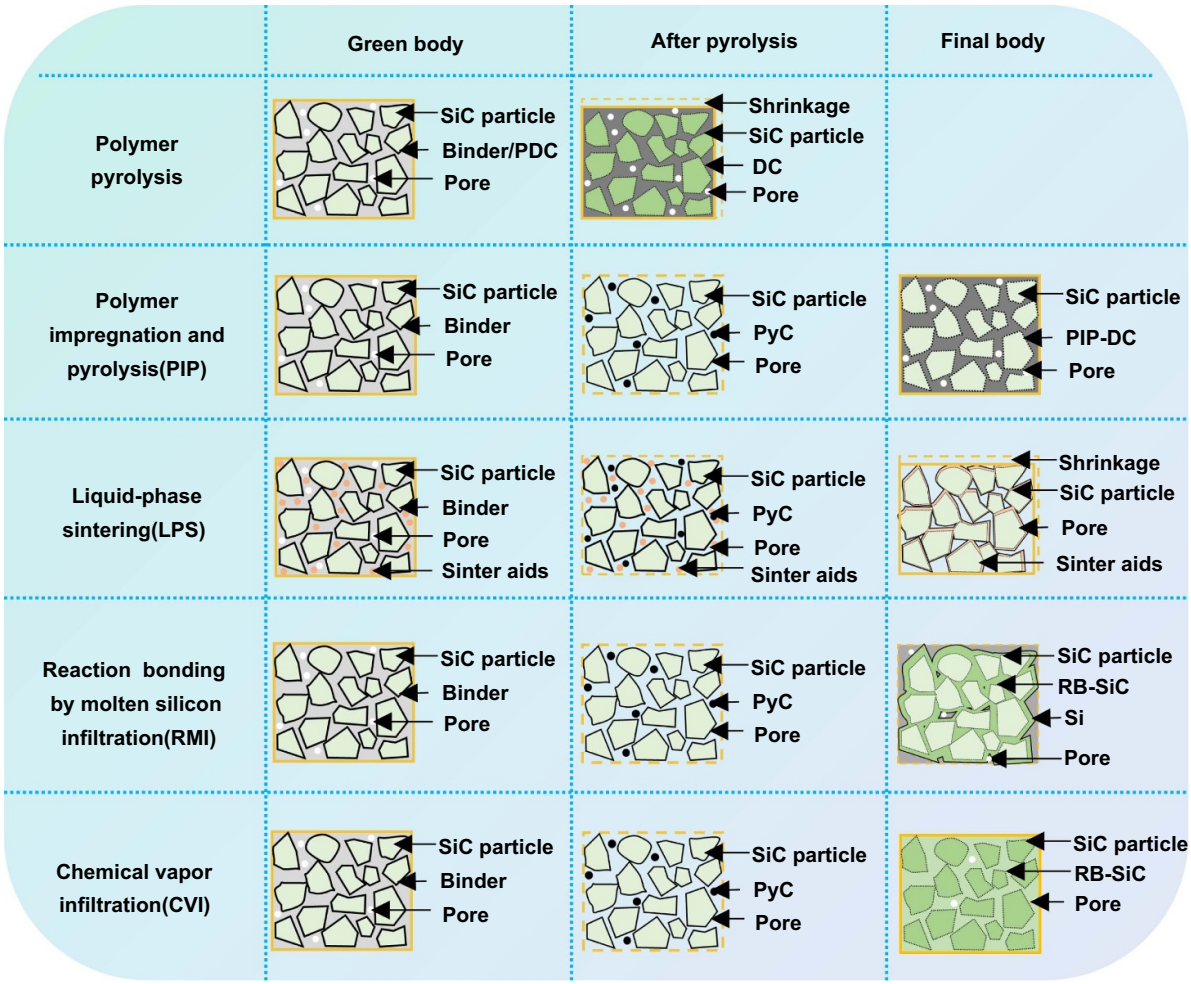


Figure 11. Sintering and densification strategies for SiC-based ceramics produced by AM (DC: (polymer)-derived ceramic, PyC: pyrolytic carbon, RB-SiC: reaction-bonded SiC).

properties that make them suitable for a variety of applications. However, further functionalization treatments are often required for specific application scenarios. For example, when SiC-based structural ceramics are used as catalyst supports, although the chemical stability of the SiC carrier is excellent, the addition of catalysts is still necessary to achieve the desired effects in catalytic applications. To meet the required functional characteristics, a catalytic coating must be applied. Mei et al.[116,117], for instance, fabricated a SiC structural ceramic catalyst support using vat photopolymerization technology. They deposited a γ-Al_2O_3 layer on the carrier surface, impregnated it with a copper-based precursor solution, and finally calcined the structure at 549.85 °C for 2 hours in nitrogen to obtain a CuZnZr/γ-Al_2O_3/SiC porous catalyst.

Similarly, to produce SiC optical mirrors, post-processing treatments such as polishing and coating are necessary to achieve the required mirror finish. For example, Takeshi et al.[118] polished SiC-based structural ceramics to produce optical mirrors with considerable specular reflectivity.

Therefore, the selection of post-processing steps for functionalization depends directly on the targeted performance. Post-processing techniques include but are not limited to, polishing, coating deposition, and others.

4. Applications of SiC ceramics fabricated by the AM method

The broad application prospects of additively manufactured SiC-based structural ceramics have attracted considerable research interest because of their lightweight and high-strength mechanical properties.

4.1. Mechanical properties and applications of SiC-based ceramics

The application of SiC-based structural ceramics greatly relies on their forming and post-processing techniques. Owing to their lightweight and high-strength mechanical properties, potential uses fall into two main categories: lightweight high-strength structural components and lightweight high-strength space mirrors. Both applications are enabled by the intrinsic lightweight and high-strength characteristics of SiC-based ceramics.

4.1.1. AM of SiC-based ceramics for aerospace applications. High-end manufacturing of SiC structural components for aerospace applications focuses on the

exceptional mechanical strength and thermal stability of the material. In 2009, Ohnabe et al.[119] reviewed the potential use of ceramic matrix composites (CMCs) in aero-engine components, particularly in hot-section parts, with SiC-based composites being a primary candidate.

For fabricating such components, integrated additive manufacturing (AM) offers a promising monolithic alternative. The AM approaches can be divided into indirect and direct forming routes. Indirect methods involve additively manufacturing a mold, such as for SiC-based turbine blades, whereas direct methods fabricate the SiC green body outright—although challenges remain in achieving precise multi-part assembly.

Following the indirect route, a resin mold produced via stereolithography has been used in a casting process combined with liquid silicon infiltration to fabricate SiC-based turbine blades[120], which produced a resin mold via stereolithography and used it in a casting process combined with liquid silicon infiltration to fabricate SiC-based turbine blades. Mechanically, with 15 wt% short carbon fibers, the SiC ceramic achieved a flexural strength of 270 MPa and a fracture toughness of 5.1 MPa·m$^{1/2}$. Through the subsequent optimization of slurry parameters, including solid loading, particle size, and fiber content, an improved SiC ceramic was developed, exhibiting a flexural strength of 350 MPa and a fracture toughness of 4.49 MPa·m$^{1/2}$ and meeting application benchmarks[121]. An optimal direct 3D printing of turbine blades remains aligned with the target application. Selecting an optimal direct 3D printing approach for the fabrication of turbine blades is closely linked to the target application envisioned. Therefore, the fabrication of aerospace SiC components via additive manufacturing demonstrates a direct correspondence between tailored mechanical properties (e.g., flexural strength above 300 MPa and fracture toughness beyond 4 MPa·m$^{1/2}$) and application requirements, where optimized process parameters enable the material to meet the stringent performance benchmarks of high-temperature, high-stress environments such as aero-engine hot sections.

4.1.2. AM of SiC-based space mirror blanks. Recent advancements in additive manufacturing show high promise for fabricating intricately shaped space mirrors, although practical implementation has yet to occur. Compared with indirect forming, direct fabrication offers more efficient routes for producing lightweight space mirrors[32,111,122,123]. Ding et al.[32] successfully manufactured a structured space mirror via vat photopolymerization by precursor infiltration and pyrolysis (PIP) (Figure 12(a)). The green body and resulting part are shown in Figure 12(b). After densification, the ceramic achieved a relative density of 93.5% (Figure 12(c)) and a flexural strength of 165.2 MPa. In a similar approach, large-sized (>500 mm) space mirrors were fabricated using vat photopolymerization with combined PIP (CPIP) and reactive melt infiltration (RMI)[122]. Microstructural analysis of a section after CPIP revealed two types of carbon: amorphous carbon with disordered stacking (Figures 12(d) and (e)) and graphitic carbon with increased micro-crystallinity (Figure 12(f)). By controlling the content of amorphous and pyrolytic carbon, the final SiC/Si composite obtained via RMI contained only 11.58% residual silicon and achieved a flexural strength of 280.09 MPa. Figures 12(g) and (h) show the front and back views of the resulting SiC mirror with a diameter exceeding 500 mm, demonstrating the feasibility of manufacturing large-scale components. To further advance practical applications, a mirror was fabricated using the same vat photopolymerization and RMI processes (Figure 12(i))[111]. It was polished to an optical finish (Figures 12(j) and (k)) while meeting structural density and strength requirements.

Beyond vat photopolymerization, Li et al.[123] employed material extrusion to fabricate a SiC mirror green body (Figure 12(l)), which was then densified via RMI (Figure 12(m)). Owing to the limited resolution of extrusion-based printing, the sintered part required polishing. After polishing, the mirror exhibited partial reflectivity (Figures 12(n) and (o)). A dense glass layer was then deposited via laser cladding onto the 3D-printed SiC surface (Figure 12(p)). Following subsequent polishing and silver coating, the mirror demonstrated excellent reflectivity, with an average reflectance exceeding 97% within the 500–800 nm wavelength range, passing application-oriented performance tests (Figure 12(q)). These studies confirm that additive manufacturing is a feasible and integrated approach for producing SiC-based space mirrors, enabling tailored solutions to meet specific requirements in strength, accuracy, and dimensions based on the characteristics of each AM process. Regarding forming methods, techniques such as SL and DIW, which possess large-format forming capabilities, are applicable. Employing the SL process, which combines large-format forming with high-precision requirements, can eliminate the need for subsequent structural component polishing, thereby offering distinct advantages. Clearly, beyond structural dimensional requirements, the degree of densification and performance characteristics are equally indispensable factors. To ensure that the polished mirror achieves a mirror-like finish, the density must exceed 99%. Generally, the results obtained through RMI impregnation prove more effective. Furthermore, the residual silicon content should be less than 10%, and the flexural strength must be at least 250 MPa.

4.2. AM of SiC-based ceramics for thermal applications

In addition to its excellent mechanical properties, silicon carbide (SiC) exhibits high thermal conductivity and a low coefficient of thermal expansion (CTE), making it an ideal material for thermal management and heat dissipation applications. Additionally, when oxidized at high temperatures, SiC forms SiC@SiO_2 core-shell composites that combine low thermal conductivity with high mechanical strength, rendering them suitable for high-temperature thermal insulation. This section provides an application-oriented review of additively manufactured SiC-based ceramics in both thermal conduction and insulation applications.

4.2.1. AM of SiC-based ceramics for heat transfer applications. With a theoretical thermal conductivity of up

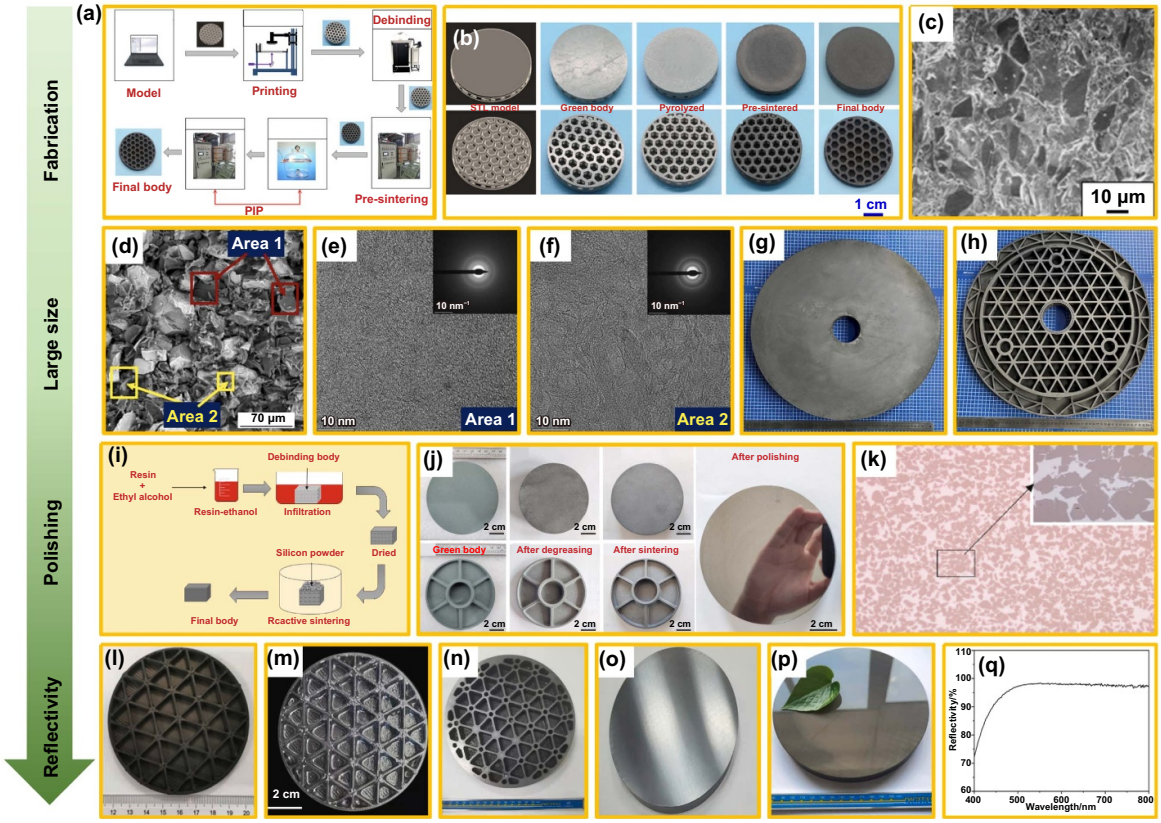


Figure 12. SiC-based ceramics for space mirror blanks based on AM. (a) Flow diagram of the manufacturing of a lightweight SiC ceramic optical mirror. (b) Photographs of a lightweight SiC ceramic optical mirror. (c) SEM image of the cross-section of a SiC-sintered sample. (a)–(c) Reprinted from[32], Copyright (2020), with permission from Elsevier. (d) Microstructure and properties of a SiC preform. (e) TEM (transmission electron microscope) image of Area 1 in (d). (f) TEM image of Area 2 in (d). (g)–(h) Large-aperture SiC mirror fabricated by the VPP and RMI techniques: (g) Top mirror surface. (h) Back-side surface. (d), (e), (g), (h) Reprinted from[122], Copyright (2024), with permission from Elsevier. (i) The debinding and RMI processes. (j) Photos of a lightweight SiC spatial optical mirror. (k) Morphology of the polished surface of an RB-SiC mirror. (i), (j) Reprinted from[111], Copyright (2021), with permission from Elsevier. (l) 3D-printed dense green body of a SiC mirror. (m) Sintered body. (n) and (o) Polished body. (p) Glass layer after polishing. (q) Reflectivity of the SiC mirror coated with a Ag film. (l)–(q) Reprinted from[123], Copyright (2022), with permission from Elsevier.

to 300 $W{\cdot}m^{-1}{\cdot}K^{-1}$, SiC-based ceramics are promising candidates for heat dissipation and thermal management structures[45,54,124,125]. As shown in Figure 13(a), the sample fabricated by the combination of BJT and CVI achieved 92% densification (Figure 13(b)), with a thermal diffusivity exceeding 0.12 $cm^2{\cdot}s^{-1}$ below 200 °C (Figure 13(c)) and a thermal conductivity above 30 $W{\cdot}m^{-1}{\cdot}K^{-1}$ (Figure 13(d))[54]. In another demonstration, a vase was fabricated using DIW (Figure 13(e)), with its surface morphology and cross-sectional microstructure compared before and after PIP in Figure 13(f)–(h)[124]. Evidently, the SiC-based ceramics produced in the aforementioned studies fall significantly short of the theoretical heat transfer coefficient values. This discrepancy stems from two primary factors: low purity of the SiC phase and high porosity. For instance, Ho et al.[45] evaluated the cooling performance of SiC-based structures, manufacturing $SiC@SiO_2/MgSO_4$ components produced via vat photopolymerization, the assembly achieved a density of (82.8 ± 3.0)% (Figure 13(i)). Owing to suboptimal purity and compactness, its thermal conductivity reached only 38.3 $W\ m^{-1}{\cdot}K^{-1}$. In the cooling tests, the SiC structure reached 79.8 °C, nearly matching the 79.3 °C of an aluminum heatsink (Figure 13(j)). Although the cross-section aluminum has higher intrinsic thermal conductivity (typically 90–250 $W{\cdot}m^{-1}{\cdot}K^{-1}$), the 3D-printed SiC structure provided a larger surface area, resulting in comparable overall heat dissipation (Figure 13(k)–(m)).

Considering the influence of secondary phases, Tang et al.[125] incorporated high-thermal-conductivity materials into SiC to form composites. As described by the Maxwell model (Figure 13(n)), the resulting diamond/SiC, carbon fiber/SiC, and pure SiC samples exhibited average thermal conductivities of approximately 7.97, 6.30, and 5.80 $W{\cdot}m^{-1}{\cdot}K^{-1}$, (Figures 13(o) and (p)), and thermal diffusivities of 6.8, 6.2, and 5.2 $cm^2{\cdot}s^{-1}$ (Figure 13(q)). The results indicate that while the introduction of other phases leads to impurities in the SiC-based ceramic particles, the incorporation of phases with high thermal conductivity has a positive effect on enhancing thermal conductivity.

Essentially, the practical thermal conductivity of additively manufactured SiC ceramics remains substantially lower than the theoretical values, primarily due to insufficient phase

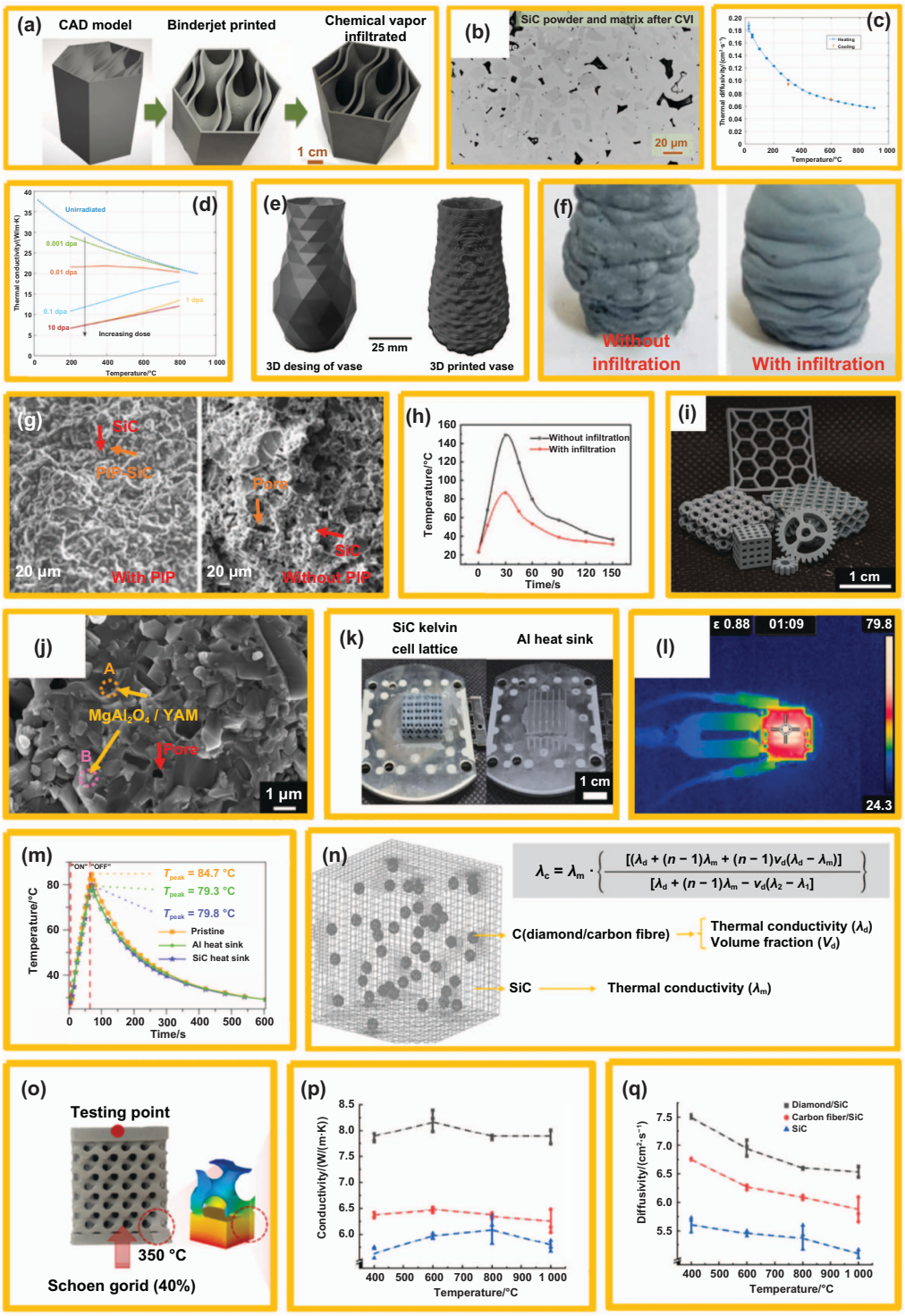


Figure 13. SiC-based structures for thermally conductive applications based on AM. (a) SiC-based thermal conduction structure manufactured using BJT and CVI processes. (b) SEM image of a printed specimen. (c) High thermal conductivity efficiency of SiC-based ceramic and its thermal conductivity coefficient. (d) Thermal conductivity of a SiC-based ceramic. (a)–(d) [54] John Wiley & Sons. Published 2019. This article is a U.S. Government work and is in the public domain in the USA. (e) SiC vase manufactured using FDM combined with PIP. (f) Comparison of SiC-based vase images before and after PIP. (g) SEM image of specimen with the formation of pores. (h) Temperature changes in heating and cooling cycles with and without infiltration conditions. (e)–(h) Reprinted with permission from[124]. Copyright (2024) American Chemical Society. (i) SiC-based heat dissipation structures fabricated by DLP with LPS. (j) Sample microstructure. (k) Printed Kelvin cell lattice and conventional aluminum heat sink adhered to the LED chip. (l) Thermal image showing the peak temperature of the LED attached with SiC heat sink. (i)–(l) Reprinted from[45], Copyright (2023), with permission from Elsevier. (m) LED chip temperature over time with SiC or Al heat sinks. (n) Maxwell model for the thermal conductivity of C/SiC. (o) Simulation of the Schoen gyroid structure for thermal insulation at 40% porosity. (p) Thermal conductivity changes as a function of temperature. (q) Thermal diffusivity of SiC, carbon fiber-reinforced SiC, and diamond-reinforced SiC as a function of temperature. (n)–(q) Reprinted from[125], Copyright (2024), with permission from Elsevier.

purity and relatively low density. The primary research focus lies in obtaining high-purity, high-density SiC-based ceramic matrices through optimized post-processing techniques. Then, enhancing thermal performance and identifying viable applications for architectured SiC thermal structures remain key for future research. Therefore, to realize the application of SiC-based ceramics by additive manufacturing in thermal insulation, the higher the level of densification is, the better the performance will be. Furthermore, the thermal conductivity must be at least equal to or exceed the minimum thermal conductivity coefficient of 90 for aluminum heat spreaders. Only then can the application value of SiC-based structures for heat conduction be preliminarily demonstrated.

4.2.2. AM of SiC-based ceramics for thermal insulation applications. In thermal insulation applications, additive manufacturing of SiC-based ceramics primarily focuses on SiC aerogels, whose thermal conductivity is as low as 0.025 $W{\cdot}m^{-1}{\cdot}K^{-1}$[126,127]. The insulation performance can be further enhanced by oxidizing SiC nanowire-based aerogels to form $SiC@SiO_2$ core-shell structures. Owing to the intrinsically low thermal conductivity of SiO_2, the resulting oxidized $SiC@SiO_2$ aerogels achieve a specific surface area of up to 600 $m^2{\cdot}g^{-1}$, a density of 40 $kg{\cdot}m^{-3}$, and a thermal conductivity as low as 0.014 $W{\cdot}m^{-1}{\cdot}K^{-1}$ at room temperature[128]. Guo et al.[129] used direct ink writing to fabricate a carbon fiber-based template, followed by high-temperature sintering at 1 500 °C to induce in-situ growth and self-assembly of SiC nanowires (Figure 14(a)), forming the SiC nanowire (SiC_{nw}) structure, as shown in Figure 14(b). This material showed a thermal conductivity as low as 0.046 $W{\cdot}m^{-1}{\cdot}K^{-1}$. Its insulation performance was clearly demonstrated by infrared imaging, where an I/O chip covered with the SiC_{nw} aerogel remained at 49.3 °C versus 86.0 °C for an exposed chip (Figure 14(c)). Further development led to modified refractory SiC nanowires (MR-SiC_{nw}) using SiO_2 and Al_2O_3 base materials[130]. Oxidation of a DIW-printed SiC_{nw} aerogel (Figure 14(d)) produced an MR-$SiC_{nw}@SiO_2$ structure (Figure 14(e)) capable of withstanding 1 000 °C and exhibiting a thermal conductivity of 0.021 $W{\cdot}m^{-1}{\cdot}K^{-1}$, highlighting the enhanced insulation from oxidation (Figure 14(f)). Separately, insulating structures were created by infiltrating SLS-printed SiC scaffolds with SiO_2 aerogel via sol-gel (Figure 14(g))[131]. Evaluation of single- and double-layer BCLC frameworks revealed that the single-layer structure had superior mechanical properties (119.41 MPa compressive strength, 2.85 GPa modulus, 2 588.41 $kJ{\cdot}m^{-3}$ energy absorption) (Figure 14(h)), whereas the double-layer structure showed better thermal insulation, reaching 701.3 °C after 1 500 s at 1 000 °C (Figure 14(i)). This provides a reliable method for manufacturing complex, load-bearing integrated thermal insulation components with significant application potential.

In general, the thermal insulation properties of SiC-based structural ceramics are manifested in two aspects: the SiC ceramic matrix provides structural strength support, while the oxidized SiO_2 delivers thermal insulation. The key lies in the equilibrium between the phase compositions.

4.3. AM of SiC-based ceramic for electromagnetic absorption

In recent years, electromagnetic wave absorption has gained increasing attention for electromagnetic shielding applications. To meet stealth operation needs, various types of components are being developed. Radar-absorbing structures (RASs) integrated with structural materials demonstrate superior comprehensive performance and broader application prospects compared to radar-absorbent coatings[132,133]. Typically, such materials incorporate wave-absorbing silicon carbide (SiC), which provides advantages in density and broadband performance over traditional electromagnetic materials[134–136]. Research on additively manufactured SiC-based electromagnetic wave-absorbing ceramics includes pure SiC[137–140], SiC composites[136,141,142], and SiC nanowire (SiC_{nw}) absorbers[143–145], covering both the GHz and THz bands.

As shown in Figure 15(a), He et al.[137] fabricated porous SiC ceramics via direct ink writing (DIW) and investigated their mechanical and electromagnetic absorption properties. The effects of the sintering temperature on the microstructure and EM wave absorption were examined. The samples sintered at 1 650 °C exhibited tightly bonded heterogeneous interfaces between the SiC particles and sintering additives (Figure 15(b)), which enhanced the interfacial polarization and increased the dielectric loss (Figure 15(c)). The absorber achieved a minimum reflection loss (RL) of −27.1 dB at a 3 mm thickness with an effective absorption bandwidth (EAB) of 3.4 GHz (Figure 15(d)). Advancing beyond material composition, structural design through powder extrusion printing enabled twisted meta-structures with an exceptional EAB of 32.87 GHz and a minimum RL of −57.15 dB, featuring notable angle insensitivity and thermal stability (Figures 15(e)–(g))[139]. Furthermore, DIW was also used to create stepped honeycomb structures, which exhibited a broad EAB of 34.64 GHz and maintained performance at high temperatures and oblique angles after PIP densification (Figures 15(h) and (i))[140].

Beyond pure-SiC structures, composite approaches have proven effective, such as growing SiC via CVD(chemical vapor deposition) on printed carbon scaffolds and adding Fe_3O_4, which achieved an RL_{min} of −48.7 dB and a stable bandwidth by tuning the conductivity (Figures 15(j)–(m))[136]. Performance has also been enhanced by leveraging the SiC nanowire morphology. In one method, composites with twisted metamaterial structures were fabricated, using carbon nanotubes to nucleate SiC_{nw} growth for increased loss, achieving an RC_{min} of −56.84 dB (Figure 15(n))[144]. In addition, a hierarchical SiC_{nw}/SiC_w structure was formed by infiltrating a binder-jetted foam, resulting in a strong RCmin of −57 dB and validating the "wire-on-sphere" design concept (Figures 15(o) and (p))[143].

The growing research interest in THz wave absorption has highlighted the strong potential of SiC-based materials for high-frequency shielding. Gyroid triply periodic minimal surface (TPMS) structures have been fabricated for this purpose by vat photopolymerization of an electrophoretically assembled SiC_w@MXene/SiOC composite

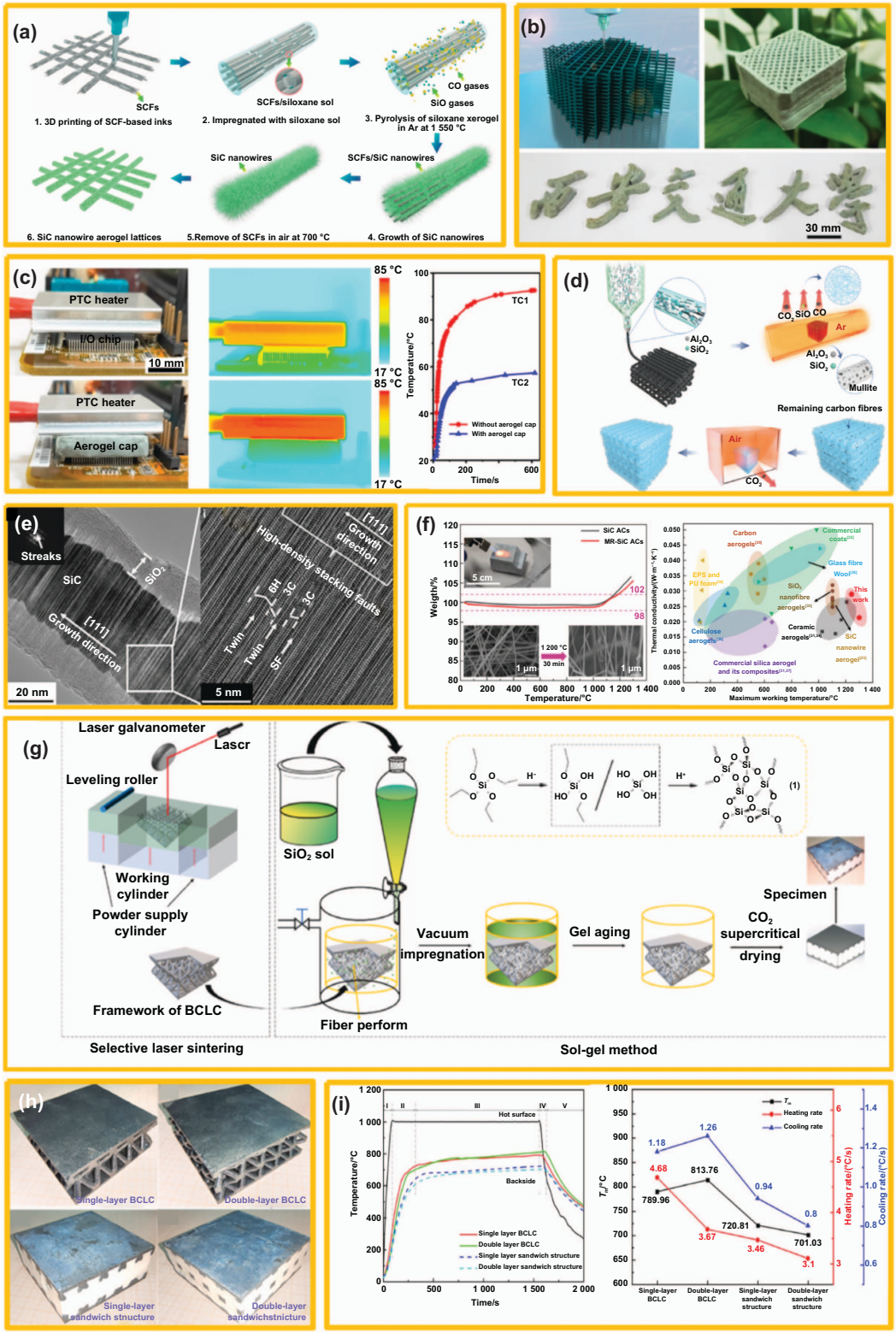


Figure 14. SiC-based structures for thermal insulation applications based on AM. (a) Schematic of 3D SiC nanowire aerogels fabrication. (b) DIW printing route and photograph of the SiC nanowire aerogel lattice. (c) Photographs of the assembled PTC heater, SiC nanowire aerogel cap, and I/O chip with infrared images showing temperature changes when the PTC heater was placed directly on the I/O chip or on the aerogel cap that buckled on the I/O chip and temperature–time curves. (a)–(c) Reprinted with permission from[129]. Copyright (2022) American Chemical Society. (d) Diagram of 3D-printed MR-SiC fabrication. (e) TEM image and corresponding electron diffraction pattern of nanowires. (f) TGA curve indicating the thermo-oxidative stability and thermal conductivity versus the maximum working temperature of insulating materials. (d)–(f) [130] John Wiley & Sons. © 2024 Wiley-VCH GmbH. (g) Schematic of the experimental process. (h) Macroscopic digital photographs of a single-layer BCLC, double-layer BCLC, single-layer sandwich structure, and double-layer sandwich structure. (i) Temperature curve for quartz lamp single-side heated test at 1 000 °C for 1 500 s with three test parameters. (g)–(i) Reprinted from[131], Copyright (2023), with permission from Elsevier.

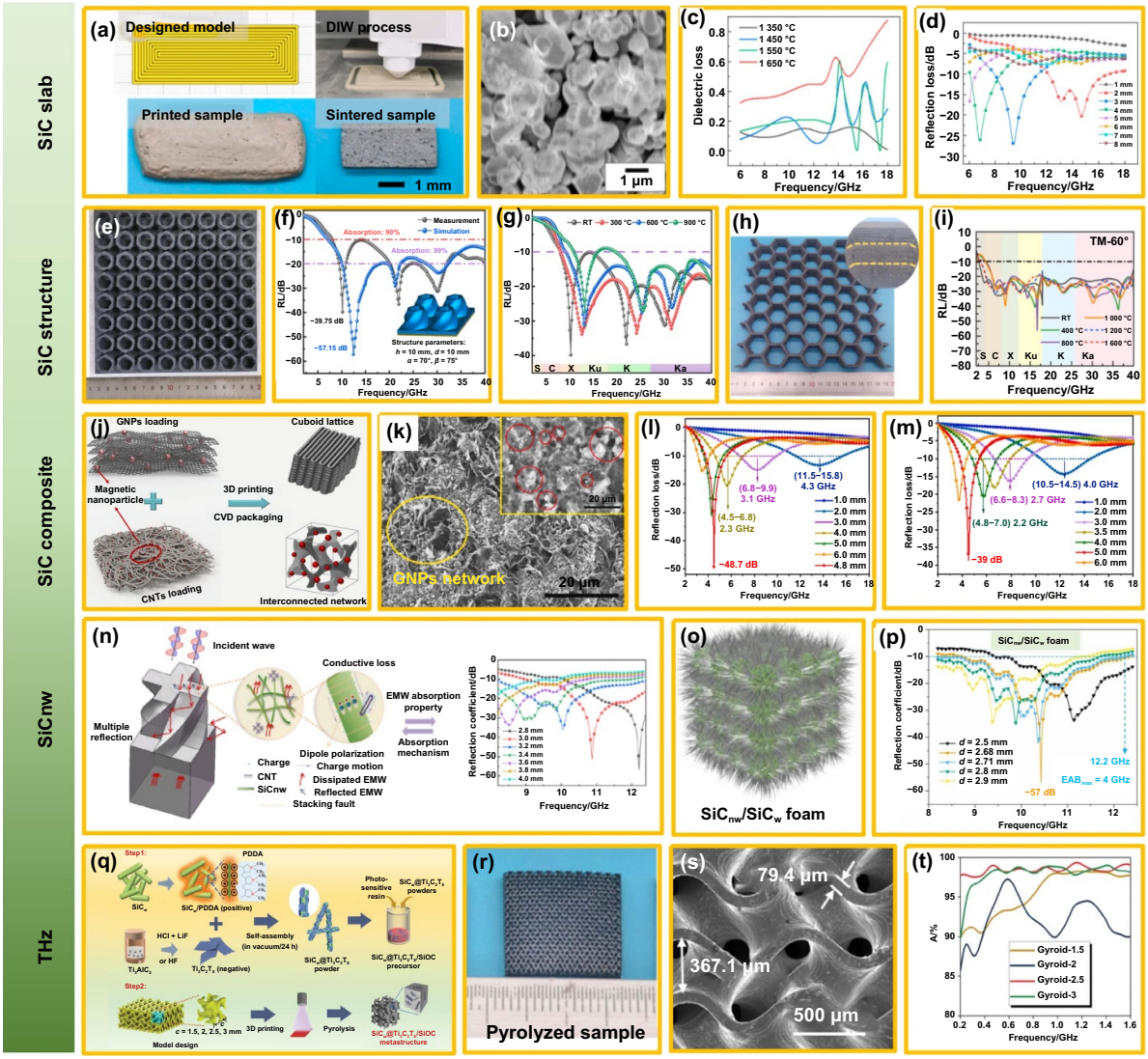


Figure 15. SiC-based structures for electromagnetic absorption applications based on AM. (a) Designed model, direct-ink-writing 3D-printing process, and images of the samples after printing and sintering. (b) Cross-sectional SEM micrographs of the porous SiC ceramics sintered at 1 650 °C. (c) Dielectric properties of the porous SiC ceramics sintered at different sintering temperatures. (d) Reflection loss for various thicknesses of porous SiC ceramics sintered at 1 650 °C. (a)–(d) Reproduced from[137]. CC BY 4.0. (e) Digital photos of the twisted torsion metamaterial. (f) Simulation and experimental RL curves for the torsion metamaterial. (g) High-temperature microwave absorption performance of twisted meta-material. (e)–(g) Reprinted from[139], Copyright (2025), with permission from Elsevier. (h) SiC honeycomb meta-structure with a graded structure. (i) Experimental RL of the SiC honeycomb metastructure in the TE at 60°incident angles. (h), (i) Reprinted from[140], Copyright (2024), with permission from Elsevier. (j) Schematic of structural evolution in the preparation processes of FGCS composites. (k) SEM image of the fracture surface of the prepared FGCS composite. (l) and (m) RL of the EMWs of as-prepared FGCS-2 before and after 400 °C annealing for 4 h in the frequency range of 2−18 GHz. (j)–(m) Reprinted from[136], Copyright (2022), with permission from Elsevier. (n) Schematic illustration of the in-situ growth of SiC nanowires@carbon nanotubes on 3D-printed metamaterial structures and the electromagnetic wave absorption mechanism. Reprinted from[144], Copyright (2021), with permission from Elsevier. (o) SiC_{nw}/SiC_w foam. (p) Room-temperature EWA performance of SiC_{nw}/SiC_w foam in the X-band at different thicknesses. (o), (p) Reprinted from[143], Copyright (2022), with permission from Elsevier. (q) Schematic illustration of the synthesis of the SiCw@$Ti_3C_2T_x$/SiOC precursor and SiC_w@MXene/SiOC meta-structure. (r) 3D-printed sample with a gyroid meta-structure after pyrolysis. (s) SEM image of the top surface of the gyroid meta-structure. (t) THz wave absorption of gyroid meta-structures with different cell sizes. (q)–(t) [142] John Wiley & Sons. © 2025 Wiley-VCH GmbH.

(Figure 15(q))[142]. Characterized by a fine wall thickness (<100 μm) and unit size (<500 μm)—much smaller than GHz absorbers—these meta-structures (1.3−2.7 mm thick) delivered excellent THz EMI shielding performance in the 0.2−1.6 THz band (Figures 15(r) and (s)), with an average shielding effectiveness (SE) ranging from 58.6 to 66.4 dB (Figure 15(t)). This work thereby offers a valuable reference for realizing highly efficient THz absorption using structurally integrated SiC ceramics.

In the application of SiC structural ceramics for absorptive purposes, distorted structures, the incorporation of magnetic phases, and the generation of whisker-like microstructures all

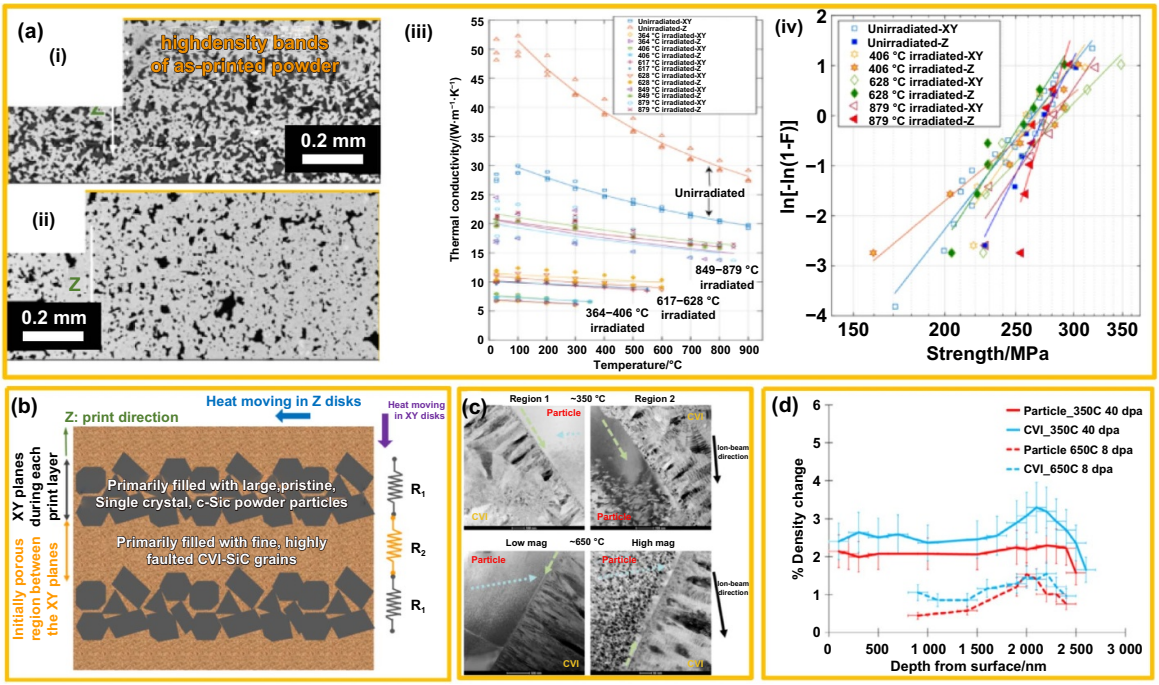


Figure 16. SiC-based structures for nuclear application based on AM. (a) Radiation resistance testing of SiC-based ceramics. (a-i) Optical image of the cross-section of a poorly infiltrated XY disk and (a-ii) cross-section of an optimally infiltrated XY disk. (a-iii) Thermal conductivity of 3D-printed SiC in the XY and Z directions before and after irradiation to 2.3 dpa at various temperatures. (a-iv) Weibull strength plot from ring-on-ring tests on 3D-printed SiC disks before and after irradiation at 2.3 dpa. (b) Heat transport in the Z direction of 3D-printed SiC. Reprinted from[146], Copyright (2021), with permission from Elsevier. (c) STEM BF images of the interface between the CVI matrix and α-SiC particles in the 5 MeV Si ion-irradiated specimens to a peak dose of 40 dpa at 350 °C and −650 °C. (d) Measured density change of depth in the α-SiC particles and CVI matrix in the ion-irradiated samples at both temperatures. Reprinted from[112], Copyright (2022), with permission from Elsevier.

yield positive effects on electromagnetic shielding. Regarding additive manufacturing technology selection, for GHz-band electromagnetic shielding, large-format forming techniques such as DIW and BJT exhibit certain advantages. Conversely, for THz-band absorptive applications, SL/DLP technologies, which combine high precision with large-format forming capabilities, have distinct advantages. Overall, the objective of additive manufacturing of SiC-based structural ceramics for absorptive applications is to achieve a large effective absorptive bandwidth (EAB) through synergistic optimization of the material and structure, resulting in integrated structural–functional components. Finally, a significant advantage of silicon carbide-based ceramic materials over other coatings or metallic materials in the field of absorptive properties lies in their stable absorptive behaviour under extreme conditions, such as high temperatures. Consequently, alongside the conclusions drawn from their fundamental absorptive behaviour (EAB) testing, assessments of their absorptive stability under such extreme conditions will serve as a distinctive advantage, demonstrating their application value.

4.4. AM of SiC-based ceramics for other applications

As a net-shaped manufacturing technology leveraging the intrinsic properties of SiC ceramics, SiC 3D printing offers significant advantages in applications requiring customized components[12,112,146–148] exceptional chemical stability[105,117,149], advanced power/energy devices[150–152] and ceramic matrix composites[153–156].

In nuclear radiation resistance applications, Terrani et al.[146] printed SiC ceramics via BJT and CVI. Pre-irradiation microstructure observations revealed layered voids within the SiC (Figure 16(a-i)), which were gradually eliminated through excessive CVI infiltration (Figure 16(a-ii)). When irradiated to 2.3 dpa at 400–850 °C, the samples maintained their strength, and the pre-existing anisotropy in thermal conductivity (Figures 16(a-iii) and (a-iv)) vanished, a change attributed to irradiation defects (Figure 16(b)). In comparison, the microscopic damage in BJT-printed SiC has been directly compared with conventional CVI-SiC under irradiation[112]. TEM characterization indicated similar defect accumulation (Figure 16(c)), and EELS (electron energy loss spectroscopy) analysis showed that radiation-induced swelling was comparable between the printed particles and the CVI matrix (Figure 16(d)), validating the nuclear-grade suitability of 3D-printed SiC. Therefore, SiC-based ceramics produced via the CVI process exhibit equivalent radiation resistance to that of SiC particles, demonstrating the potential of the process for radiation-resistant applications[157].

Owing to its high chemical stability, SiC is also employed as a catalyst support. Fabricated via DIW, SiC scaffolds with regular pores have been used to develop a novel MSR microreactor[149]. After conversion to porous ceramics, the

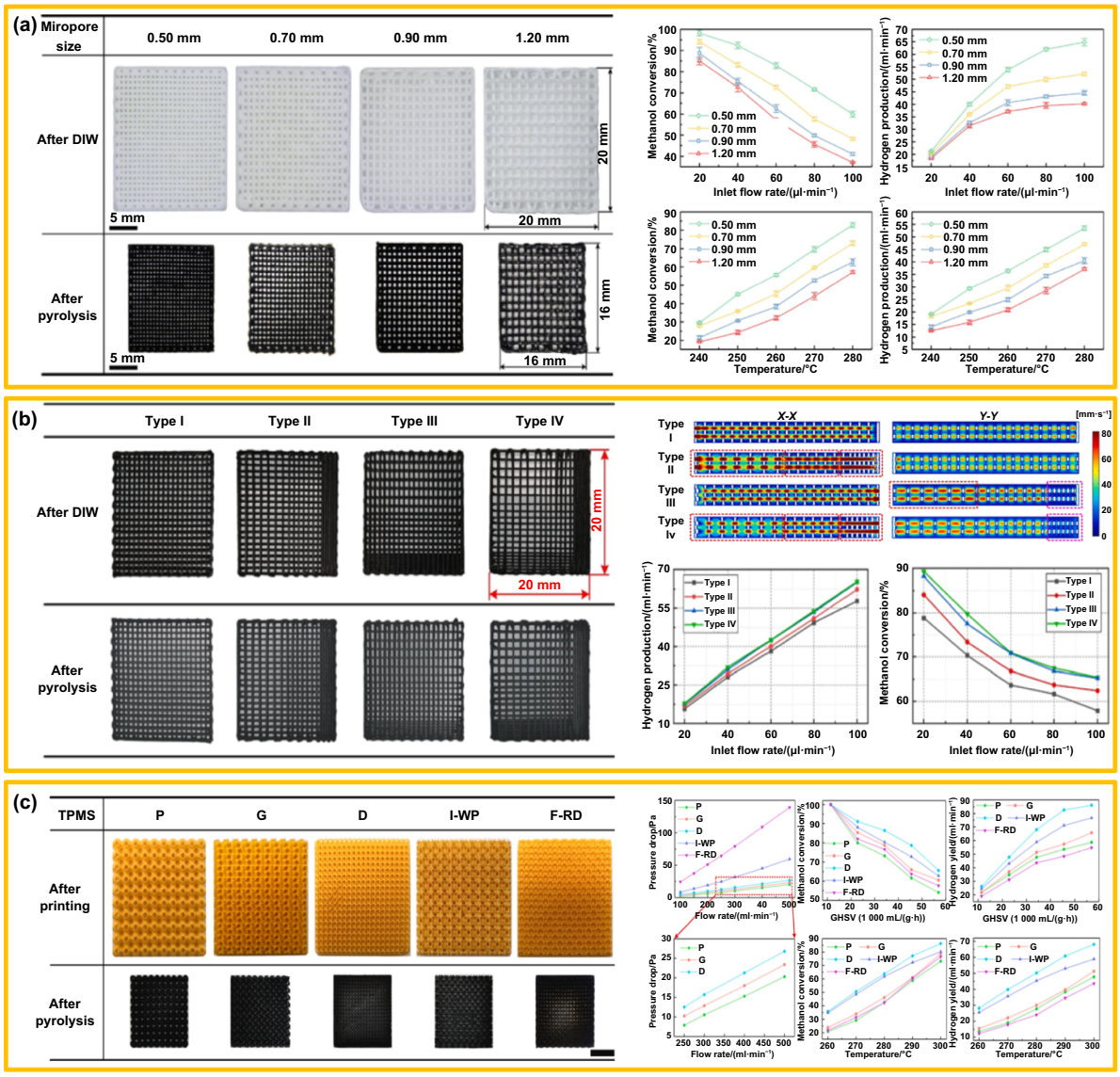


Figure 17. SiC-based structures for catalytic application based on AM. (a) DIW-printed SiC scaffolds with different pore sizes and hydrogen production performances of the microreactor based on printed SiC scaffolds. Reprinted from[149], Copyright (2022), with permission from Elsevier. (b) SiC catalyst supports, simulation of flow velocity, and hydrogen production/methanol conversion of the microreactor with different catalyst supports. Reprinted from[105], Copyright (2023), with permission from Elsevier. (c) DLP-printed SiC scaffolds with different structures and hydrogen production performances of the microreactor based on different SiC structures. Reprinted from[117], Copyright (2023), with permission from Elsevier.

scaffolds with smaller pores yielded maximum hydrogen production and demonstrated stable performance over 24 hours (Figure 17(a)). Optimization through numerical modelling revealed that a graded pore size distribution, determined via the steepest ascent method, could significantly improve reactor performance by reducing the pressure drop and increasing methanol conversion (Figure 17(b))[105]. Beyond the structural complexity limits of DIW, fabrication via DLP has enabled the production of SiC-based TPMS structures for catalysis (Figure 17(c))[117]. Comparative evaluation of the five TPMS types identified the D surface as the most effective. These advancements highlight the significant potential of architectured SiC supports fabricated by additive manufacturing for catalytic applications[158–162]. Comparing catalytic performance of SiC-based ceramic carriers produced via DIW and DLP processes, it is evident that DLP-manufactured carriers demonstrate superior efficacy. This advantage stems from the technology's superior structural design flexibility and manufacturing precision. Consequently, focusing on additive manufacturing techniques with high structural design freedom and precision for preparing catalytic carriers will represent a key future development direction.

Beyond catalysis, additively manufactured SiC ceramics have been explored for diverse applications. For instance, they have been employed to manufacture volumetric receivers for solar thermal power plants (STPPs)[150]. Three optimized structures were tested under high-flux solar irradiation in a solar concentrator simulating STPP operating conditions.

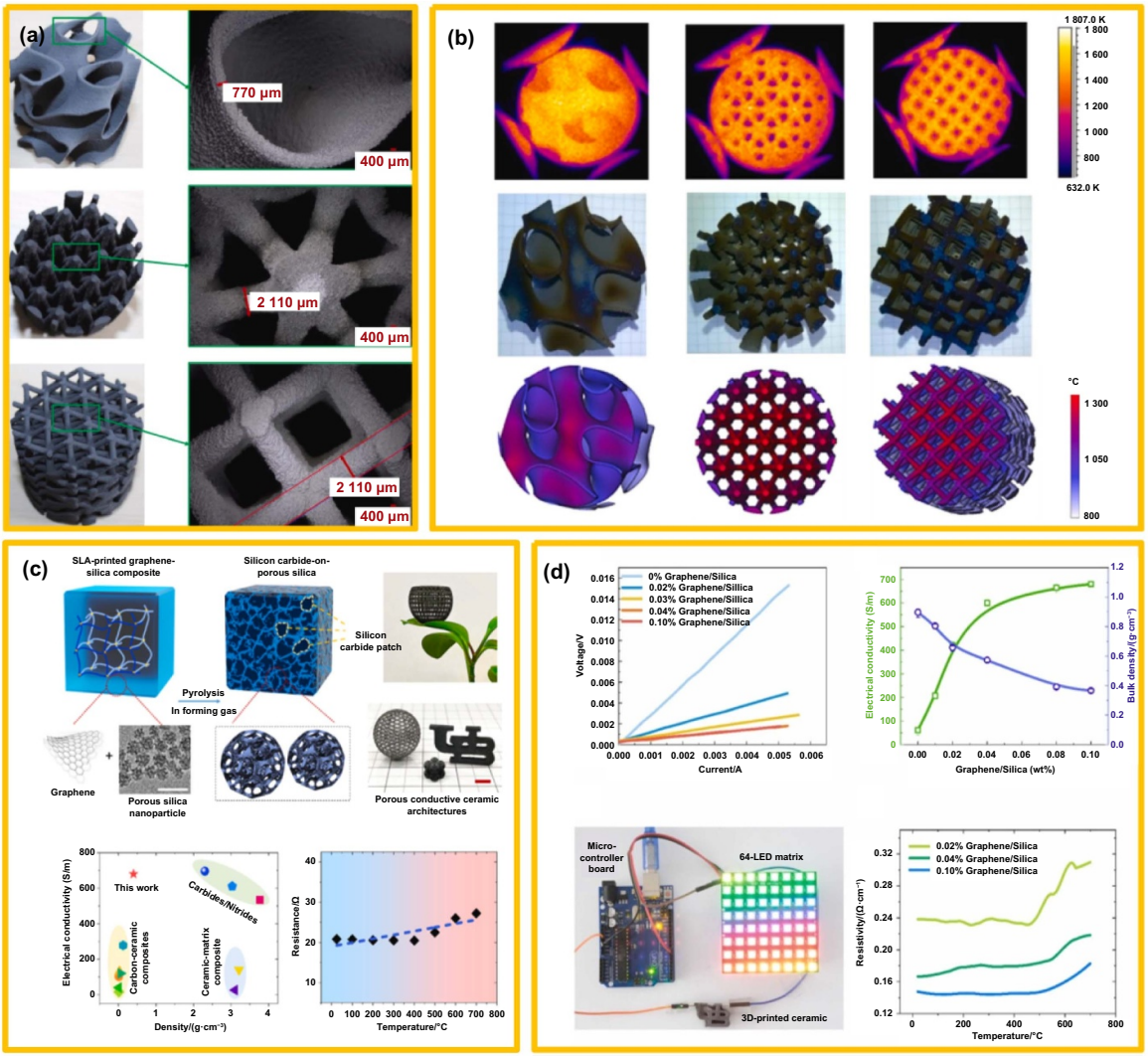


Figure 18. SiC-based structures for electrical application based on AM. (a) Three printed structures for analysis. (b) Top: black body equivalent temperature images at the front for an air flow equal to 1 $g \cdot s^{-1}$. Middle: pictures of the structures after the tests. Bottom: numerical results. Reprinted from[150], Copyright (2021), with permission from Elsevier. (c) 3D printing of electrically conductive SiC and its performance. (d) Conductive characterization of the 3D-printed SiC structure. Reprinted from[152], Copyright (2022), with permission from Elsevier.

These uniquely shaped structures achieved a maximum average outlet air temperature of 859.85 °C (Figures 18(a) and (b)), withstanding temperatures up to 1 226.85 °C, demonstrating the possibility of using additively manufactured SiC for solar energy devices.

In the field of flexible electronics, a polydimethylsiloxane (PDMS)/SiC functionally graded substrate with variable stiffness has been proposed[151]. The graded PDMS/SiC substrate exhibited the smallest resistance change rate under deformation, proving the protective effect of its design compared to pure PDMS variants. Furthermore, composite approaches have been used to create materials for high-temperature electronics. A uniform conductive network was established within a SiC ceramic scaffold by infiltrating graphene[152]. Established a uniform conductive network by infiltrating graphene into a SiC ceramic scaffold. The resulting composite achieved an electrical conductivity of up to 1 000 $S \cdot m^{-1}$ and a thermal conductivity ranging from 62 to 88 $mW \cdot m^{-1} \cdot K^{-1}$, indicating a promising pathway for such applications (Figures 18(c) and (d)). Evidently, in the field of additive manufacturing for SiC-based ceramic electrical applications, the approach remains primarily demand-driven, with no established mainstream development trends or patterns having emerged.

Compared with conventional methods, both the AM processes and post-treatment equipment—including sintering, densification, and reinforcement—directly influence the manufacturing precision, strength, and density of SiC ceramics. However, achieving high density and strength remains a challenge for SiC ceramics, regardless of the AM technology used.

Table 2 compares key performance parameters such as the density, flexural strength, modulus, dimensional accuracy, and build size of SiC ceramics fabricated via different AM techniques. Dimensional accuracy is represented by the smallest printable feature size, while the build size is based on reported parts. These data summarize the current state of research on

Table 2. Comparison of the relative density and strength of SiC-based ceramics fabricated by additive manufacturing techniques with different printing accuracies and printing areas.

No	Technology	Material	Sintering method	Relative density /%	Bending Strength /MPa	Printing accuracy/mm	Printing area/mm^2	Application	References
1	Traditional	SiC/SiC_w	Hot pressing	96.6	710 ± 17	/	/	/	[163]
2	Traditional	SiC	Pressureless sintering	98	531 ± 38	/	/	/	[164]
3	Traditional	SiC/SiC_w	Reactive sintering	90	290 ± 12	/	/	/	[165]
4	Traditional	SiC/SiC_w	Pressureless sintering	96	540	/	/	/	[166]
5	TPP	SiOC	Pressureless sintering	/	/	0.000 34	0.071	/	[16]
6	TPP	SiOC	Pressureless sintering	/	/	0.000 2	0.002 25	/	[13]
7	TPP	SiOC	Pressureless sintering	/	/	0.000 349	0.025	/	[14]
8	SL/DLP	SiC	PIP	93.50	165.2	0.2	1 963	Optical mirror	[32]
9	SL/DLP	SiC	LPS	78.2 ± 1.36	210.4 ± 10.3	/	/	/	[42]
		SiC	PIP	82.6 ± 0.48	184.2 ± 8.5	/	/	/	
		SiC/Si	RMI(LSI)	96.2 ± 0.32	210.4 ± 10.3	/	/	/	
10	SL/DLP	SiC	PIP	94.3	217.36	/	/	Wave absorption	[138]
11	SL/DLP	SiC/Cf/Si	RMI(LSI)	/	262.6	0.023	2 500	/	[24]
12	SL/DLP	SiC/Si	RMI(LSI)	99.8	234.8	0.05	2 000	/	[167]
13	SL/DLP	SiC/Si	RMI	99.5	280.09	0.1	196 230	Optical mirror	[122]
14	SL/DLP	SiC/Si	RMI	93.5	460	/	/	/	[23]
15	SL/DLP	$SiC/Y_xAl_yO_z$	LPS	93.9	225.3 ± 13.6	0.025	1 500	/	[31]
16	SL/DLP	$SiC/SiC\text{-}O_x$-20 M	LPS	82.8 ± 3.1	155 ± 20	0.02	400	Heat dissipation	[45]
17	BJT	SiC/Si	PIP and RMI(LSI)	>99	277 ± 10.2	0.05	3 000	/	[168]
18	BJT	SiC/Si	PIP	>99	205.24 ± 4.15	0.3	10 000	Optical mirror	[169]
19	BJT	SiC	CVI	91.3	297	/	>10 000	Heat dissipation	[54]
20	BJT	SiC	CVI	/	274	/	/	Nuclar application	[146]
21	SLS	$SiC/TiSi_2/Si$	RMI(LSI)	99	434.6	/	/	/	[170]
22	SLS	$SiC/C_f/Si$	RMI(LSI)	>95	249 ± 17.0	1.5	>2 025	/	[58]
23	SLS	SiC	PIP	>97	201	/	/	/	[56]
24	SLS	SiC/C	PIP	>97	202.1	/	/	Friction components	[171]
25	DIW	SiC/C_{cf}	LPS	77.36 ± 3.08	113.17 ± 20.79	>2.2	>900	/	[172]
26	DIW	SiC/C_{cf}	RMI(LSI)	99.65	253.63	>0.5	>1 000	/	[173]
27	DIW	SiC/Si	RMI(LSI)	99.7	229	>0.8	>1 600	Heat dissipation	[174]
28	DIW	SiC/Si	RMI(LSI)	/	337.4	>0.65	>2 500	Optical mirror	[175]
29	FDM	$SiC/C_{cf}/Si$	RMI(LSI)	>95	387	>1	>48 400	Optical mirror	[176]
30	FDM	$SiC/C_{cf}/Si$	PIP and RMI(LSI)	>95	398	/	>57 600	/	[177]
31	FDM	SiC/Si	RMI(LSI)	>95	310.41 ± 39.32	>2	>10 000	Optical mirror	[123]
32	FDM	SiC/C_f	PIP	92.61	212.74	/	/	/	[178]

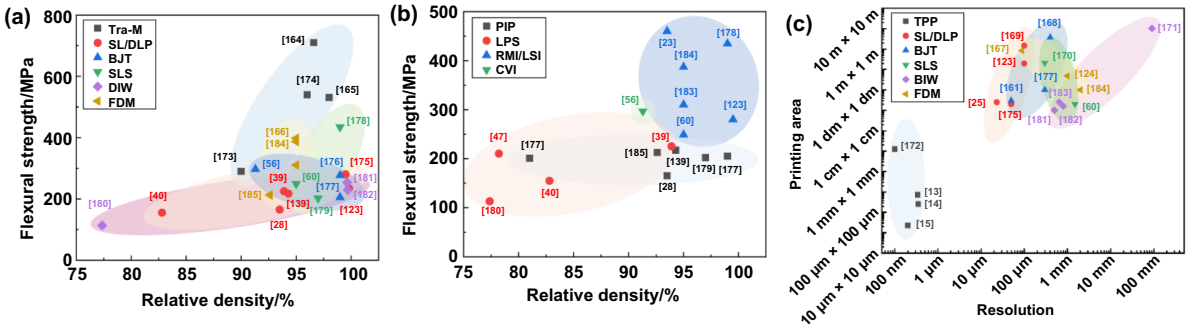


Figure 19. Comparison of SiC ceramics in different additive manufacturing technologies or different densification methods. (a) Comparison of the relative density and mechanical properties of SiC ceramics produced by different additive manufacturing technologies. (b) Comparison of the relative density and mechanical properties of SiC ceramics obtained using different densification methods. (c) Relationship between the printing area and printing resolution for SiC ceramics fabricated using different additive manufacturing technologies. (Tra-M: Traditional Method).

the strength and accuracy of AM-fabricated SiC ceramics. This comparative framework provides critical benchmarks for selecting and optimizing AM techniques based on specific performance requirements.

Figure 19(a) compares the mechanical properties and density of SiC ceramics fabricated via traditional and AM methods. Ceramics made by conventional methods generally exhibit flexural strengths exceeding 300 MPa[163,164]. For instance, Dong et al.[163] achieved a strength of 710 MPa using hot-pressed sintering with SiC whisker (SiC_w) reinforcement, ultrafine nano-powders, and polycarbosilane (PCS) as a sintering aid. However, replicating such performance with AM processes remains difficult, and the mechanical properties of AM-fabricated SiC ceramics still lag behind those of their traditionally manufactured counterparts. Therefore, advancing AM processes to close this performance gap is a central research objective in the field.

Among AM processes, vat photopolymerization (SL/DLP) is limited in terms of slurry solid loading and raw material form, yet it can produce SiC ceramics with flexural strengths above 300 MPa. Direct ink writing (DIW) is limited by the solid content and interparticle bonding stability, making significant improvements challenging, but the limited organic content in the feedstock reduces the presence of defects in the sintered ceramic body. In contrast, fused deposition modeling (FDM) offers better material adaptability and green body cohesion, enabling SiC ceramics reinforced with continuous fibers to approach 400 MPa in strength[177]. This highlights the importance of aligning the selected AM technique with the target property profile, where fiber reinforcement strategies offer a clear route to higher strength.

Post-processing densification significantly affects the mechanical and structural properties of SiC ceramics. Figure 19(b) shows that reactive melt infiltration (RMI) provides high densification and superior mechanical properties, making it a key method for producing high-strength SiC ceramics, followed by chemical vapor infiltration (CVI). Precursor infiltration and pyrolysis (PIP) is effective for densification but still underperforms compared to RMI and CVI. Liquid-phase sintering (LPS) results in relatively low densification because of porosity formation during binder melt-phase condensation of SiC particles, leading to poor mechanical performance. However, the LPS process is facile and economical. Depending on the specific application requirements, the chosen densification method may vary. For instance, when SiC structural ceramics are selected as load-bearing components[121–123] or thermal carriers for heat dissipation[45,54,105,124], density is the paramount consideration. Consequently, densification processes such as PIP and RMI, which achieve high levels of densification, are typically preferred. Conversely, for applications such as catalysis[105,117,149] or heat insulation[126,127], where component density requirements are less stringent, densification methods like liquid-phase sintering or one-step pyrolysis may be selected. Thus, the selection of a densification strategy must be a balanced decision, prioritizing either ultimate performance or process efficiency based on the component's functional role.

For practical applications, dimensional accuracy and build size are critical factors in addition to the mechanical performance. Recent studies focus on small demonstration structures, and equipment specifications are provided for reference (FDM[179], BJT[180], SL/DLP[181], SLS[182], DIW[183], and TPP[184]). As summarized in Figure 19(c), two-photon polymerization (TPP) offers the highest precision, reaching sub-micron resolution, followed by SL/DLP. DIW offers the largest build size but the lowest resolution, additionally, the extruder can be mounted on a robotic arm to further expand the printing envelope and diversify the achievable architectures. However, the printing accuracy and build size are inversely related. Processes such as SL/DLP, SLS, FDM, and BJT—capable of sub-millimeter precision and relatively large build volumes—are currently the mainstream choices for engineering ceramic components. This inherent trade-off necessitates a careful, application-driven selection of the AM process to best satisfy the competing demands of detail, scale, and throughput.

Figure 20 provides a comprehensive schematic summary of additive manufacturing for silicon carbide throughout the text, covering everything from raw material forms and types to additive manufacturing techniques, densification processes,

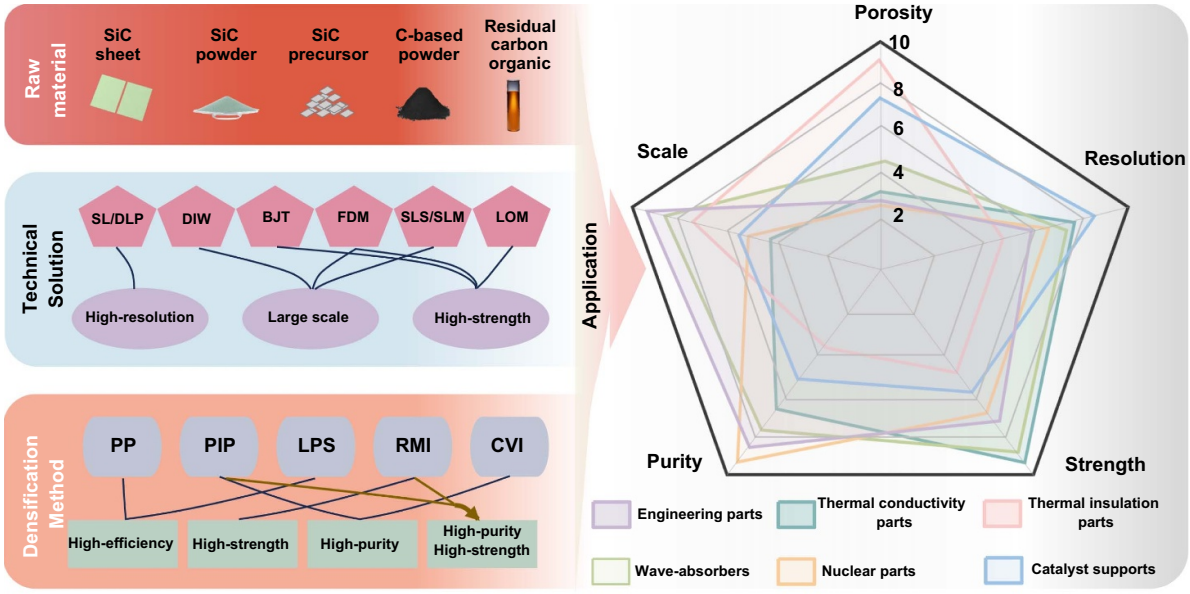


Figure 20. Schematic diagram of AM-SiC from raw material to its applications.

and finally application requirements. The selection of raw materials for SiC additive manufacturing is extensive and includes SiC sheets, powders, precursors, carbon-based particles, and residual carbon-containing organic compounds. This broad material system accommodates diverse additive manufacturing techniques, each possessing distinct characteristics. Nevertheless, achieving the integrated production of high-precision, large-format, and high-strength SiC-based ceramics remains challenging. Within densification processes, options range from the efficiency-focused PP and LPS techniques to the high-strength RMI measures. For high-purity SiC-based ceramics, PIP and CVI dominate. Balancing high strength and purity may necessitate combining high-purity PIP approaches with high-strength RMI solutions. Finally, practical applications differentiate between various directions based on purity, strength, format size, porosity, and printing precision. For engineering structural components, low porosity, high strength, and large-scale manufacturing are clearly essential for reliability. For thermal conduction components, high-purity and low-porosity achieve superior thermal conductivity, making them the preferred choice for heat transfer and dissipation requirements. Conversely, thermal insulation structures require lower purity but higher porosity to reduce thermal conductivity and enhance insulation performance. Structural absorptive SiC ceramics demand high precision and strength: precision ensures design and manufacturing consistency, with dimensions significantly affecting absorption frequency bands, while strength addresses specific load-bearing requirements. In nuclear applications, high-purity SiC guarantees radiation resistance, with load-bearing capacity and precision requirements considered subsequently. For catalytic carriers, precision demands are elevated for catalytic flow channels, particularly in smaller microfluidic applications, whilst other factors may be moderately accommodated. Consequently, by aligning with the specific requirements of each SiC structural application, an appropriate manufacturing pathway can be selected through the strategic combination of additive manufacturing processes and post-processing techniques, leveraging their respective characteristics.

5. Conclusions and outlooks

Additive manufacturing (AM) has the potential to significantly transform the advanced ceramics industry, opening up new opportunities such as increased design flexibility, tailored microstructures, material grading, mold-free fabrication, and economical low-volume production. Compared to conventional methods, AM enables the fabrication of SiC components with sub-micron to tens-of-micron accuracy and large build sizes. AM of SiC shows broad potential in aerospace, high-strength space parts, heat exchangers, RF absorption, chemical catalysis, and other applications, providing a solid research foundation for further industrial adoption. The current state of research and its challenges are summarized as follows:

(1) Although most additive manufacturing techniques can be applied to the fabrication of SiC-based ceramics, forming SiC-based ceramics via the TPP method remains challenging. This finding indicates that significant hurdles persist in the micro- and nano-scale (<1 μm) fabrication of SiC materials.
(2) Additive manufacturing of SiC-based ceramics faces challenges such as shrinkage and phase purity during the transition from green body to ceramic. The fundamental cause of this phenomenon lies in the difficulty of achieving a solid-phase SiC content exceeding 60% in the raw material, regardless of the additive manufacturing technique employed. The sintering densification process is accompanied by significant shrinkage rates. Although methods

such as RMI and CVI can reduce the shrinkage rate of SiC-based ceramics to less than 10%, they introduce issues with phase purity. Consequently, whether it be substantial shrinkage rates or unstable phase purity, these factors constitute the primary constraints on the structural precision and performance of additive-manufactured SiC-based ceramics.

(3) SiC-based ceramics produced via additive manufacturing techniques face inherent trade-offs between manufacturing precision and build volume. While processes such as BJT and DIW offer high design freedom and scalability for large build volumes, they typically exhibit lower manufacturing accuracy. Conversely, SL/DLP technologies deliver superior dimensional accuracy but often suffer from limitations in achievable part dimensions.

(4) In practical applications, SiC-based ceramics produced via additive manufacturing serve diverse purposes, including load-bearing structural components, electromagnetic shielding, and radiation resistance. While structural elements such as SiC space mirrors exhibit a high degree of maturity, other applications continue to face challenges concerning purity, strength, and large-scale manufacturing.

Based on the above summary and challenges, compared to traditional processing techniques, additive manufacturing of silicon carbide structural ceramics still exhibits a significant gap in application maturity, leaving ample scope for subsequent research and development. Key issues and development prospects include the following:

(1) Although macroscale AM approaches for SiC have been extensively studied, offering reduced lead times and greater geometric freedom compared to traditional methods—as-printed parts often exhibit insufficient density, flexural strength, and other properties for extreme environments such as aerospace[6,185]. Lengthy post-densification treatments are still required, making it a key research goal to achieve near-net-shaped SiC ceramics with service-ready properties in a single manufacturing step.

(2) Micro-scale AM of SiC lags significantly behind that of other materials. While nanoscale AM of SiOC materials have been successfully 3D-printed at the nanoscale, SiC precursors are still limited to macro features[13,16,186,187]; thus, developing new material systems compatible with the micro/nano AM of SiC is crucial for the cross-scale manufacturing of SiC components.

(3) Current AM technologies face challenges in balancing accuracy, efficiency, and build volume for large-scale components[188]. To meet the growing demand for large-sized and functional SiC ceramics, the integration of multiple AM techniques (hybridization) is crucial for fabricating monolithic components with fine structural features[189,190].

(4) Multi-material (MM) 3D printing shows great potential in metamaterials, flexible electronics, and other multifunctional applications owing to its ability to integrate materials with different properties in a single structure[191]. Designing gradient and composite SiC-based ceramics through this approach is highly significant for practical applications[192].

(5) The development of single-step AM processes to produce defect-free, fully dense SiC ceramic bodies would represent a key advancement, and it may become achievable in the near future. AM processes such as DIW and LOM can achieve high strength but possess limited geometric freedom. Overcoming process compatibility barriers and developing strategies for strengthening and toughening SiC via SL/DLP, SLS, and BJT is crucial to produce high-strength, high-toughness, and high-precision SiC ceramics. Combining approaches such as toughening coating deposition[193], toughening phase infiltration[194], oriented toughening phase formation[195], and 2D material interlayer compositing[196], and the addition of both short fibers[197] and continuous fibers[177] may eventually enable the integrated AM of SiC ceramics with superior overall properties.

Acknowledgments

This work was financially supported by National Natural Science Foundation of China (52475387), Innovation Team of the Department of Education of Guangdong Province (2025KCXTD038), Guangdong Basic and Applied Basic Research Foundation (2024A1515010049), and Shenzhen Science and Technology Programs (JCYJ20250909154017263, SGCX20250526143506009).

ORCID iDs

Muhammad Irfan Hussain 0000-0001-8203-6231
Zhangwei Chen 0000-0002-5301-3740

References

[1] Eom J-H, Kim Y-W and Raju S. 2013. Processing and properties of macroporous silicon carbide ceramics: a review. *J. Asian Ceram. Soc.* **1**, 220–242.
[2] Ramírez-rico J, Singh M, Zhu D and Martínez-fernández J. 2017. High-temperature thermal conductivity of biomorphic SiC/Si ceramics. *J. Mater. Sci.* **52**, 10038–10046.
[3] Boretti A and Castelletto S. 2024. A perspective on 3D printing of silicon carbide. *J. Eur. Ceram. Soc.* **44**, 1351–1360.
[4] He R, Zhou N, Zhang K, Zhang X, Zhang L, Wang W and Fang D. 2021. Progress and challenges towards additive manufacturing of SiC ceramic. *J. Adv. Ceram.* **10**, 637–674.
[5] Cho Y et al. 2022. Fabrication methods for microscale 3D structures on silicon carbide. *Int. J. Precis. Eng. Manuf.* **23**, 1477–1502.
[6] Padture N P. 2016. Advanced structural ceramics in aerospace propulsion. *Nat. Mater.* **15**, 804–809.
[7] Liu K, Shi Y, Li C, Hao L, Liu J and Wei Q. 2014. Indirect selective laser sintering of epoxy resin-Al_2O_3 ceramic powders combined with cold isostatic pressing. *Ceram. Int.* **40**, 7099–7106.

[8] Chen Z et al. 2019. 3D printing of ceramics: a review. *J. Eur. Ceram. Soc.* **39**, 661–687.
[9] Hwa L C, Rajoo S, Noor A M, Ahmad N and Uday M B. 2017. Recent advances in 3D printing of porous ceramics: a review. *Curr. Opin. Solid State Mater. Sci.* **21**, 323–347.
[10] Grzybowski A and Pietrzak K. 2013. Maria Goeppert-Mayer (1906–1972): two-photon effect on dermatology. *Clin. Dermatol.* **31**, 221–225.
[11] Sun H-B and Kawata S. 2004. Two-photon photopolymerization and 3D lithographic microfabrication. *NMR • 3D Analysis • Photopolymerization* (eds Sun H-B, Kawata S) (Springer Berlin Heidelberg, Berlin, Heidelberg) pp 169–273.
[12] Chaudhary R P, Parameswaran C, Idrees M, Rasaki A S, Liu C, Chen Z and Colombo P. 2022. Additive manufacturing of polymer-derived ceramics: materials, technologies, properties and potential applications. *Prog. Mater. Sci.* **128**, 100969.
[13] Bauer J, Crook C, Izard A G, Eckel Z C, Ruvalcaba N, Schaedler T A and Valdevit L. 2019. Additive manufacturing of ductile, ultrastrong polymer-derived nanoceramics. *Matter* **1**, 1547–1556.
[14] Konstantinou G et al. 2020. Additive micro-manufacturing of crack-free PDCs by two-photon polymerization of a single, low-shrinkage preceramic resin. *Addit. Manuf.* **35**, 101343.
[15] Pham T A, Kim D P, Lim T W, Park S-H, Yang D-Y and Lee K-S. 2006. Three-dimensional SiCN ceramic microstructures via nano-stereolithography of inorganic polymer photoresists. *Adv. Funct. Mater.* **16**, 1235–1241.
[16] Brigo L, Schmidt J E M, Gandin A, Michieli N, Colombo P and Brusatin G. 2018. 3D nanofabrication of SiOC ceramic structures. *Adv. Sci.* **5**, 1800937.
[17] Kim I and Yoon Y-J. 2024. Digital light processing 3D printing of porous ceramics: a systematic analysis from a debinding perspective. *Addit. Manuf.* **93**, 104409.
[18] Zanchetta E, Cattaldo M, Franchin G, Schwentenwein M, Homa J, Brusatin G and Colombo P. 2016. Stereolithography of SiOC Ceramic Microcomponents. *Adv. Mater.* **28**, 370–376.
[19] Eckel Z C, Zhou C, Martin J H, Jacobsen A J, Carter W B and Schaedler T A. 2016. Additive manufacturing of polymer-derived ceramics. *Science* **351**, 58–62.
[20] de Hazan Y and Penner D. 2017. SiC and SiOC ceramic articles produced by stereolithography of acrylate modified polycarbosilane systems. *J. Eur. Ceram. Soc.* **37**, 5205–5212.
[21] Zhong X, Pei X, Miao Y, He L and Huang Q. 2017. Accelerating the crosslinking process of hyperbranched polycarbosilane by UV irradiation. *J. Eur. Ceram. Soc.* **37**, 3263–3270.
[22] Chen J, Wang Y, Pei X, Bao C, Huang Z, He L and Huang Q. 2020. Preparation and stereolithography of SiC ceramic precursor with high photosensitivity and ceramic yield. *Ceram. Int.* **46**, 13066–13072.
[23] Chen R, Lian Q, He X, Wang J and Li D. 2021. A stereolithographic diamond-mixed resin slurry for complex SiC ceramic structures. *J. Eur. Ceram. Soc.* **41**, 3991–3999.
[24] Zhang H, Yang Y, Hu K, Liu B, Liu M and Huang Z. 2020. Stereolithography-based additive manufacturing of lightweight and high-strength Cf/SiC ceramics. *Addit. Manuf.* **34**, 101199.
[25] Ding G, He R, Zhang K, Xia M, Feng C and Fang D. 2020. Dispersion and stability of SiC ceramic slurry for stereolithography. *Ceram. Int.* **46**, 4720–4729.
[26] Zou W, Yang P, Lin L, Li Y and Wu S. 2022. Improving cure performance of Si3N4 suspension with a high refractive index resin for stereolithography-based additive manufacturing. *Ceram. Int.* **48**, 12569–12577.
[27] Chang H, Tang J, Guo X, Zhu Y, Liu M, Wei Y, Hu X, Huang Z, Chen Z and Yang Y. 2023. Stereolithography-based additive manufacturing of RB-SiC ceramics by a two-step sintering method. *Ceram. Int.* **49**, 1085–1091.
[28] Tang J, Chang H, Guo X, Liu M, Wei Y, Huang Z and Yang Y. 2022. Preparation of photosensitive SiO_2/SiC ceramic slurry with high solid content for stereolithography. *Ceram. Int.* **48**, 30332–30337.
[29] Qu P, Liang G, Hamza M, Mo Y, Jiang L, Luo X, Liu Z, Liu C, Lou Y and Chen Z. 2024. 3D printing of high-purity complex SiC structures based on stereolithography. *Ceram. Int.* **50**, 23763–23774.
[30] Cao J, Idrees M, Tian G, Liu J, Xiong S, Yuan J, Wang P, Liu Z, Liu C and Chen Z. 2021. Complex SiC-based structures with high specific strength fabricated by vat photopolymerization and one-step pyrolysis. *Addit. Manuf.* **48**, 102430.
[31] Shi Z A, Wu J M, Fang Z Q, Tian C, Wang Q-W, Mao C, Fu L-X and Shi Y-S. 2024. Investigation of curing behavior and mechanical properties of SiC ceramics prepared by vat photopolymerization combined with pressureless liquid-phase sintering using Al_2O_3-coated SiC powder. *Addit. Manuf.* **79**, 103942.
[32] Ding G, He R, Zhang K, Zhou N and Xu H. 2020. Stereolithography 3D printing of SiC ceramic with potential for lightweight optical mirror. *Ceram. Int.* **46**, 18785–18790.
[33] Tang J, Guo X, Chang H, Hu K, Shen Z, Wang W, Liu M, Wei Y, Huang Z and Yang Y. 2021. The preparation of SiC ceramic photosensitive slurry for rapid stereolithography. *J. Eur. Ceram. Soc.* **41**, 7516–7524.
[34] Cao J, Miao K, Xiong S, Su F, Gao D, Lin X, Liu Z, Wang P, Liu C and Chen Z. 2022. 3D printing and in situ transformation of SiCnw/SiC structures. *Addit. Manuf.* **58**, 103053.
[35] Shi Z-A, Wu J-M, Fang Z-Q and SHI Y-S. 2023. Influence of high-temperature oxidation of SiC powders on curing properties of SiC slurry for digital light processing. *J. Adv. Ceram.* **12**, 169–181.
[36] Guo X, Tang J, Chang H, Zhu Y, Wei Y, Hu X, Huang Z and Yang Y. 2023. Application of SiO_2-coated SiC powder in stereolithography and sintering densification of SiC ceramic composites. *Ceram. Int.* **49**, 25016–25024.
[37] He R, Ding G, Zhang K, Li Y and Fang D. 2019. Fabrication of SiC ceramic architectures using stereolithography combined with precursor infiltration and pyrolysis. *Ceram. Int.* **45**, 14006–14014.
[38] Ding G, He R, Zhang K, Xie C, Wang M, Yang Y and Fang D. 2019. Stereolithography-based additive manufacturing of gray-colored SiC ceramic green body. *J. Am. Ceram. Soc.* **102**, 7198–7209.
[39] Xing H, Zou B, Wang X, Hu Y, Huang C and Xue K. 2020. Fabrication and characterization of SiC whiskers toughened Al2O3 paste for stereolithography 3D printing applications. *J. Alloys Compd.* **828**, 154347.
[40] Hu C et al. 2021. Effect of SiC powder on the properties of SiC slurry for stereolithography. *Ceram. Int.* **47**, 12442–12449.
[41] Yang J, Yu R, Li X, He Y, Wang L, Huang W and Jiao J. 2021. Silicon carbide whiskers reinforced SiOC ceramics through digital light processing 3D printing technology. *Ceram. Int.* **47**, 18314–18322.
[42] Bai X, Ding G, Zhang K, Wang W, Zhou N, Fang D and He R. 2021. Stereolithography additive manufacturing and sintering approaches of SiC ceramics. *Open Ceram.* **5**, 100046.
[43] Qu P, Liang G, Hussain M I, Hanif M, Hamza M, Huang K, Lou Y and Chen Z. 2025. Low-temperature fabrication of high-specific strength SiC-based ceramics via photopolymerization 3D printing with controllable anisotropy. *Int. J. Extreme Manuf.* **7**, 055002.
[44] Shi Z A, Wu J M, Fang Z Q, Mao C, Fu L-X, Wang Q-W, Yang S-L, Zhang J-X and Shi Y-S. 2024. Particle surface

oxidation modification and particle gradation strategy for the preparation of high-strength SiC ceramics via vat photopolymerization. *Addit. Manuf.* **84**, 104118.
[45] Ho T Y K et al. 2023. Realization of vat photopolymerisation of dense SiC ceramics with SiO2/MgSO4 coated submicron powders for efficient heat dissipation. *Addit. Manuf.* **73**, 103664.
[46] Shi Z-A, Wu J-M, Mao C, Fu L-X, Yang S-L, Zhang J-X and Shi Y-S. 2025. Effect of SiO_2/AlOOH double-coated SiC powders on the properties of SiC ceramics by vat photopolymerization. *J. Eur. Ceram. Soc.* **45**, 116933.
[47] Dong H, Carr W W and Morris J F. 2006. An experimental study of drop-on-demand drop formation. *Phys. Fluids* **18**, 072102.
[48] Mott M and Evans J R G. 2001. Solid freeforming of silicon carbide by inkjet printing using a polymeric precursor. *J. Am. Ceram. Soc.* **84**, 307–313.
[49] Wadhwa A, Benavides-guerrero J, Gratuze M, Bolduc M and Cloutier S G. 2024. All screen printed and flexible silicon carbide NTC thermistors for temperature sensing applications. *Materials* **17**, 2489.
[50] Moon J, Caballero A C, Hozer L, Chiang Y-M and Cima M J. 2001. Fabrication of functionally graded reaction infiltrated SiC–Si composite by three-dimensional printing (3DP™) process. *Mater. Sci. Eng.* **298**, 110–119.
[51] Fu Z, Schlier L, Travitzky N and Greil P. 2013. Three-dimensional printing of SiSiC lattice truss structures. *Mater. Sci. Eng.* **560**, 851–856.
[52] Lv X, Ye F, Cheng L, Fan S and Liu Y. 2019. Fabrication of SiC whisker-reinforced SiC ceramic matrix composites based on 3D printing and chemical vapor infiltration technology. *J. Eur. Ceram. Soc.* **39**, 3380–3386.
[53] Baux A, Goillot A, Jacques S, Heisel C, Rochais D, Charpentier L, David P, Piquero T, Chartier T and Chollon G. 2020. Synthesis and properties of macroporous SiC ceramics synthesized by 3D printing and chemical vapor infiltration/deposition. *J. Eur. Ceram. Soc.* **40**, 2834–2854.
[54] Terrani K, Jolly B and Trammell M. 2020. 3D printing of high-purity silicon carbide. *J. Am. Ceram. Soc.* **103**, 1575–1581.
[55] Lv X, Ye F, Cheng L, Fan S and Liu Y. 2019. Binder jetting of ceramics: powders, binders, printing parameters, equipment, and post-treatment. *Ceram. Int.* **45**, 12609–12624.
[56] Jin L, Zhang K, Xu T, Zeng T and Cheng S. 2018. The fabrication and mechanical properties of SiC/SiC composites prepared by SLS combined with PIP. *Ceram. Int.* **44**, 20992–20999.
[57] Tan W K, Kuwana T, Yokoi A, Kawamura G, Matsuda A and Muto H. 2021. Electrostatically assembled SiC–Al_2O_3 composite particles for direct selective laser sintering. *Adv. Powder Technol.* **32**, 2074–2084.
[58] Zhu W, Fu H, Xu Z, Liu R, Jiang P, Shao X, Shi Y and Yan C. 2018. Fabrication and characterization of carbon fiber reinforced SiC ceramic matrix composites based on 3D printing technology. *J. Eur. Ceram. Soc.* **38**, 4604–4613.
[59] Liu K et al. 2024. Failure mechanisms of lightweight high strength Si/SiC non-uniform lattice structures by SLS/RMI. *Ceram. Int.* **50**, 35615–35626.
[60] Liu T, Chen Z, Yang L, Wen G, Xiong L, Sun C and Liu K. 2024. Additive manufacturing of high-performance CCF/SiC composites under dual protection. *Ceram. Int.* **50**, 11158–11166.
[61] Gong L, Wu H, Zhang H, Zeng S, Gao A, Li L, Li S, Ji Y and Ye X. 2024. Preparation of graphite/silicon carbide based on SLS/LSI and study of properties. *Mater. Sci. Eng. B* **309**, 117666.
[62] Yang Y, Zeng T, Liang Z, Li D, Xu G, Wang X and Cheng S. 2024. Effect of graphite content on the microstructure and mechanical properties of SLS-based RB-SiC ceramics. *Ceram. Int.* **50**, 22858–22864.
[63] Yang L, Wen G, Liu T, Xiong L, Yuan Z, Chen Z, Liu K, Sun C, Huang R and Kou Z. 2024. Enhancing mechanical properties of selectively laser sintered SiC/Si composites printed using electrostatic spraying microspheres with fine particles. *Ceram. Int.* **50**, 3556–3565.
[64] Friedel T, Travitzky N, Niebling F, Scheffler M and Greil P. 2005. Fabrication of polymer derived ceramic parts by selective laser curing. *J. Eur. Ceram. Soc.* **25**, 193–197.
[65] Shishkovsky I, Yadroitsev I, Bertrand P and Smurov I. 2007. Alumina–zirconium ceramics synthesis by selective laser sintering/melting. *Appl. Surf. Sci.* **254**, 966–970.
[66] Wei C, Chueh Y-H, Zhang X, Huang Y, Chen Q and Li L. 2019. Easy-to-remove composite support material and procedure in additive manufacturing of metallic components using multiple material laser-based powder bed fusion. *J. Manuf. Sci. Eng.* **141**, 071002.
[67] Cesarano J. 1998. A review of robocasting technology. *MRS Online Proc. Library*. vol 542, pp 133–139.
[68] Larson C M, Choi J J, Gallardo P A, Henderson S W, Niemack M D, Rajagopalan G and Shepherd R F. 2016. Direct ink writing of silicon carbide for microwave optics. *Adv. Eng. Mater.* **18**, 39–45.
[69] Chen H, Wang X, Xue F, Huang Y, Zhou K and Zhang D. 2018. 3D printing of SiC ceramic: direct ink writing with a solution of preceramic polymers. *J. Eur. Ceram. Soc.* **38**, 5294–5300.
[70] Xiong H, Chen H, Chen Z, Xiong X, Zhang D and Zhou K. 2020. 3D-SiC decorated with SiC whiskers: chemical vapor infiltration on the porous 3D-SiC lattices derived from polycarbosilane-based suspensions. *Ceram. Int.* **46**, 6234–6242.
[71] Xiong H, Chen H, Zhao L, Huang Y, Zhou K and Zhang D. 2019. SiCw/SiCp reinforced 3D-SiC ceramics using direct ink writing of polycarbosilane-based solution: microstructure, composition and mechanical properties. *J. Eur. Ceram. Soc.* **39**, 2648–2657.
[72] Xia Y, Lu Z, Cao J, Miao K, Li J and Li D. 2019. Microstructure and mechanical property of Cf/SiC core/shell composite fabricated by direct ink writing. *Scr. Mater.* **165**, 84–88.
[73] Lu Z, Xia Y, Miao K, Li S, Zhu L, Nan H, Cao J and Li D. 2019. Microstructure control of highly oriented short carbon fibres in SiC matrix composites fabricated by direct ink writing. *Ceram. Int.* **45**, 17262–17267.
[74] Zhao L, Wang X, Xiong H, Zhou K and Zhang D. 2021. Optimized preceramic polymer for 3D structured ceramics via fused deposition modeling. *J. Eur. Ceram. Soc.* **41**, 5066–5074.
[75] Mei H, Yan Y, Feng L, Dassios K G, Zhang H and Cheng L. 2019. First printing of continuous fibers into ceramics. *J. Am. Ceram. Soc.* **102**, 3244–3255.
[76] Deng Y, Ma L, Pei X, Huang Q and Huang Z. 2024. Free radical-initiated direct ink writing of liquid polycarbosilane slurry and its conversion into SiC ceramic parts with low shrinkage. *Ceram. Int.* **50**, 51252–51259.
[77] Huang W, Wang Y, Ning Z, Mao S, Xue Z, Zhu Y, Tao Q, Lan S and Yao R. 2023. Design of lightweight and antioxidant SiCnws/SiC(Mox, rGO) nanocomposite from molybdenum-modified precursors for aerospace vehicle components. *Ceram. Int.* **49**, 25998–26014.
[78] Liu H, Mei D, Yu S, Qian S and Wang Y. 2023. Direct ink writing of chopped carbon fibers reinforced polymer-derived SiC composites with low shrinkage and high strength. *J. Eur. Ceram. Soc.* **43**, 235–244.
[79] Kemp J W, Diaz A A, Malek E C, Croom B P, Apostolov Z D, Kalidindi S R, Compton B G and Rueschhoff L M. 2021. Direct ink writing of ZrB_2-SiC chopped fiber ceramic composites. *Addit. Manuf.* **44**, 102049.

[80] Spoerk M, Savandaiah C, Arbeiter F, Traxler G, Cardon L, Holzer C and Sapkota J. 2018. Anisotropic properties of oriented short carbon fibre filled polypropylene parts fabricated by extrusion-based additive manufacturing. *Composites A* **113**, 95–104.
[81] Zhou Z, Salaoru I, Morris P and Gibbons G J. 2018. Additive manufacturing of heat-sensitive polymer melt using a pellet-fed material extrusion. *Addit. Manuf.* **24**, 552–559.
[82] Liu W, Wu N and Pochiraju K. 2018. Shape recovery characteristics of SiC/C/PLA composite filaments and 3D printed parts. *Composites A* **108**, 1–11.
[83] Ferreira R T L, Amatte I C, Dutra T A and Bürger D. 2017. Experimental characterization and micrography of 3D printed PLA and PLA reinforced with short carbon fibers. *Composites B* **124**, 88–100.
[84] Taylor S L, Ibeh A J, Jakus A E, Shah R N and Dunand D C. 2018. NiTi-Nb micro-trusses fabricated via extrusion-based 3D-printing of powders and transient-liquid-phase sintering. *Acta Biomater.* **76**, 359–370.
[85] Putra N E, Leeflang M A, Minneboo M, Taheri P, Fratila-apachitei L E, Mol J M C, Zhou J and Zadpoor A A. 2021. Extrusion-based 3D printed biodegradable porous iron. *Acta Biomater.* **121**, 741–756.
[86] Sahay R, Nayak R, Naik N and Tambrallimath V. 2021. Influence of silicon carbide reinforcement on mechanical behavior of 3D printed polymer composites. *Mater. Today Proc.* **46**, 5991–5996.
[87] Kulkarni A, Sorarù G D and Pearce J M. 2020. Polymer-derived SiOC replica of material extrusion-based 3-D printed plastics. *Addit. Manuf.* **32**, 100988.
[88] Hammoud F, Lecourt J, Bilot C and Manière C. 2025. Pressureless sintering of 3D printed SiC filaments at 2200 °C: impact of coarsening, debinding atmosphere, residual carbon and anisotropy. *Prog. Addit. Manuf.* **10**, 10111–10121.
[89] Li S, Zhang H, Han Y, Lu Z, Miao K, Wang Z and Li D. 2023. Thermally assisted extrusion-based 3D printing of continuous carbon fiber-reinforced SiC composites. *Composites A* **172**, 107593.
[90] Li S et al. 2025. Fabrication of bamboo-inspired continuous carbon fiber-reinforced SiC composites via dual-material thermally assisted extrusion-based 3D printing. *J. Mater. Sci. Technol.* **208**, 92–103.
[91] Dermeik B and Travitzky N. 2020. Laminated object manufacturing of ceramic-based materials. *Adv. Eng. Mater.* **22**, 2000256.
[92] Weisensel L, Travitzky N, Sieber H and Greil P. 2004. Laminated object manufacturing (LOM) of SiSiC composites. *Adv. Eng. Mater.* **6**, 899–903.
[93] Windsheimer H, Travitzky N, Hofenauer A and Greil P. 2007. Laminated object manufacturing of preceramic-paper-derived Si?SiC composites. *Adv. Mater.* **19**, 4515–4519.
[94] Travitzky N, Windsheimer H, Fey T and Greil P. 2008. Preceramic paper-derived ceramics. *J. Am. Ceram. Soc.* **91**, 3477–3492.
[95] Chen R, Lian Q, Li D, He X, Wang S and Zhuang J. 2021. Stereolithographic additive manufacturing diamond/SiC composites with high thermal conductivity for electronic 3D-packaging applications. *Ceram. Int.* **47**, 14009–14020.
[96] Hussain M I, Xia M, Ren X, Shen Z, Jamil M and Ge C. 2025. Recent advances in photopolymerization 3D printing of alumina-ceramic. *Prog. Nat. Sci.: Mater. Int.* **35**, 1–30.
[97] Liu H, Xiao F and Gao Y. 2025. SiC powder binder jetting 3D printing technology: a review of high-performance SiC-based component fabrication and applications. *Appl. Sci.* **15**, 6488.
[98] Feng K, Sun J, Zhao W, Heng Y, Mao Y and Wei Q. 2025. An aqueous-based carbon black binder and post-treatment for enhanced binder jetting of SiC ceramics. *J. Eur. Ceram. Soc.* **45**, 117111.
[99] Qu P et al. 2021. Inkjet printing additively manufactured multilayer SOFCs using high quality ceramic inks for performance enhancement. *Addit. Manuf.* **48**, 102394.
[100] Wang X, Xiong D and Chen Z. 2023. Effective post-processing strategies of inkjet-printed ceramic cathodes for improved fuel cell performance. *Ceram. Int.* **49**, 40593–40600.
[101] Zhu N, Zhang L, Wen G and Hou Y. 2023. Effect of SiC whiskers on the mechanical properties of polymer-derived ceramics prepared by digital light processing and its strengthening and toughening mechanism. *J. Alloys Compd.* **968**, 171852.
[102] Tang J, Chang H, Guo X, Liu M, Wei Y, Huang Z and Yang Y. 2022. Preparation of carbon fiber-reinforced SiC ceramics by stereolithography and secondary silicon infiltration. *Ceram. Int.* **48**, 25159–25167.
[103] Chen Z, Li J, Liu C, Liu Y, Zhu J and Lao C. 2019. Preparation of high solid loading and low viscosity ceramic slurries for photopolymerization-based 3D printing. *Ceram. Int.* **45**, 11549–11557.
[104] Gao C, Chen J, Huang C, Liao S, Peng L and Huang Z. 2025. Pressureless solid-state sintering of SiC ceramics prepared by material extrusion 3D printing. *Ceram. Int.* **51**, 32660–32670.
[105] Qian S, Liu H, Wang Y and Mei D. 2023. Structural optimization of 3D printed SiC scaffold with gradient pore size distribution as catalyst support for methanol steam reforming. *Fuel* **341**, 127612.
[106] Huang Z, Liu L Y, Yuan J, Guo H, Wang H, Ye P, Du Z, Zhao Y, Zhang H and Gan C L. 2023. Stereolithography 3D printing of Si3N4 cellular ceramics with ultrahigh strength by using highly viscous paste. *Ceram. Int.* **49**, 6984–6995.
[107] Zhang L, Huang J, Xiao Z, He Y, Liu K, He B, Xiang B, Zhai J and Kong L. 2022. Effects of debinding condition on microstructure and densification of alumina ceramics shaped with photopolymerization-based additive manufacturing technology. *Ceram. Int.* **48**, 14026–14038.
[108] Besisa D H A, Ewais E M M, Ahmed Y M Z, Elhosiny F I, Fend T and Kuznetsov D V. 2018. Investigation of microstructure and mechanical strength of SiC/AlN composites processed under different sintering atmospheres. *J. Alloys Compd.* **756**, 175–181.
[109] Zhang K, Chen Y, Weng L, Cheng S, Yu S and Zeng T. 2024. Fabrication of dense Cf/SiC ceramic matrix composites using 3D printing and PIP with short carbon fibre as a toughening material. *Virtual Phys. Prototyp.* **19**, e2425381. (In German)
[110] Liu K, Wang J, Wu T and Sun H. 2020. Effects of carbon content on microstructure and mechanical properties of SiC ceramics fabricated by SLS/RMI composite process. *Ceram. Int.* **46**, 22015–22023.
[111] Li W, Cui C, Bao J, Zhang G, Li S and Wang G. 2021. Properties regulation of SiC ceramics prepared via stereolithography combined with reactive melt infiltration techniques. *Ceram. Int.* **47**, 33997–34004.
[112] Lach T G, Coq A G L, Linton K D, Terrani K A and Byun T S. 2022. Characterization of radiation damage in 3D printed SiC. *J. Nucl. Mater.* **559**, 153459.
[113] Liu C-Y, Tuan W-H and Chen S-C. 2013. Ballistic performance of liquid-phase sintered silicon carbide. *Ceram. Int.* **39**, 8253–8259.
[114] Yeom J-A, Kim Y-W, Jung W K, Cheong D-I and Kang E S. 2023. Pressureless sintering of SiC ceramics with improved specific stiffness. *J. Eur. Ceram. Soc.* **43**, 3941–3949.
[115] Das D, Kim G-D, Oh Y and Kim Y-W. 2024. Effects of boron source on properties of pressureless solid-state sintered silicon carbide ceramics. *J. Eur. Ceram. Soc.* **44**, 5380–5390.

[116] Wang Y, Yu S, Mei D and Liu H. 2022. Development of a centrifugal coating method to load catalyst washcoat onto porous substrates with high uniformity and adhesive strength. *Surf. Coat. Technol.* **434**, 128204.
[117] Liu H, Mei D, Qian S and Wang Y. 2023. Vat photopolymerization of polymer-derived SiC ceramic with triply period minimal surface structure for hydrogen production. *Addit. Manuf.* **73**, 103694.
[118] Takeshi N. 2014. Development of CMC turbine parts for Aaero engines.
[119] Ohnabe H, Masaki S, Onozuka M, Miyahara K and Sasa T. 1999. Potential application of ceramic matrix composites to aero-engine components. *Composites A* **30**, 489–496.
[120] Lu Z L, Lu F, Cao J W, Li D C, Lian Y Y, Miao K and Jing H. 2013. Fabricating hollow turbine blades using short carbon fiber-reinforced SiC composite. *Int. J. Adv. Manuf. Technol.* **69**, 417–425.
[121] Lu Z L, Lu F, Cao J W and Li D C. 2014. Manufacturing properties of turbine blades of carbon fiber-reinforced sic composite based on stereolithography. *Mater. Manuf. Process.* **29**, 201–209.
[122] Li W, Cui C, Li S, Zhang G, Jin B, Bao J, Guo C, Zhang Y, Liu B and Wang G. 2024. Vat photopolymerization of large-aperture high performance SiC mirror through multiphase carbon infiltration modification. *Addit. Manuf.* **85**, 104160.
[123] Li F-F, Ma N-N, Chen J, Zhu M, Chen W-H, Huang C-C and Huang Z-R. 2022. SiC ceramic mirror fabricated by additive manufacturing with material extrusion and laser cladding. *Addit. Manuf.* **58**, 102994.
[124] Das M et al. 2024. Strengthening SiC ceramic structural integrity made via 3D printing with pyrolysis and precursor infiltration. *ACS Appl. Eng. Mater.* **2**, 2549–2558.
[125] Tang D, Gao T, Chen H, Tian M, He M and Xu S. 2024. Structure optimization and heat dissipation performance of additive-manufactured diamond/SiC and carbon fiber/SiC TPMS structural panel. *J. Manuf. Process.* **127**, 589–598.
[126] Lu D, Su L, Wang H, Niu M, Xu L, Ma M, Gao H, Cai Z and Fan X. 2019. Scalable fabrication of resilient SiC nanowires aerogels with exceptional high-temperature stability. *ACS Appl. Mater. Interfaces* **11**, 45338–45344.
[127] Su L, Wang H, Niu M, Fan X, Ma M, Shi Z and Guo S-W. 2018. Ultralight, recoverable, and high-temperature-resistant SiC nanowire aerogel. *ACS Nano* **12**, 3103–3111.
[128] Su L, Wang H, Niu M, Dai S, Cai Z, Yang B, Huyan H and Pan X. 2020. Anisotropic and hierarchical SiC@SiO_2 nanowire aerogel with exceptional stiffness and stability for thermal superinsulation. *Sci. Adv.* **6**, eaay6689.
[129] Guo P, Su L, Peng K, Lu D, Xu L, Li M and Wang H. 2022. Additive manufacturing of resilient SiC nanowire aerogels. *ACS Nano* **16**, 6625–6633.
[130] Miao M, Yin J, Mao Z, Chen Y and Lu J. 2024. 3D-printed mullite-reinforced SiC-based aerogel composites. *Small* **20**, 2401742.
[131] Mei H, Li H, Jin Z, Li L, Yang D, Liang C, Cheng L and Zhang L. 2023. 3D-printed SiC lattices integrated with lightweight quartz fiber/silica aerogel sandwich structure for thermal protection system. *Chem. Eng. J.* **454**, 140408.
[132] Sun D, Zou Q, Wang Y, Wang Y, Jiang W and Li F. 2014. Controllable synthesis of porous Fe3O4@ZnO sphere decorated graphene for extraordinary electromagnetic wave absorption. *Nanoscale* **6**, 6557–6562.
[133] Wang Z et al. 2018. Ultralight, highly compressible and fire-retardant graphene aerogel with self-adjustable electromagnetic wave absorption. *Carbon* **139**, 1126–1135.
[134] Liu C, Yu D, Kirk D W and Xu Y. 2017. Electromagnetic wave absorption of silicon carbide based materials. *RSC Adv.* **7**, 595–605.
[135] Lan X, Liang C, Wu M, Wu N, He L, Li Y and Wang Z. 2018. Facile synthesis of highly defected silicon carbide sheets for efficient absorption of electromagnetic waves. *J. Phys. Chem. C* **122**, 18537–18544.
[136] You X, Dai G, Deng R, Zhang T, Song L, Zhang X, Ding Y, Yang J and Dong S. 2022. Fabrication of high-performance electromagnetic wave absorbing SiC composites reinforced by 3D printed carbon-based nanonetwork with Fe3O4 nanoparticles. *Addit. Manuf.* **55**, 102855.
[137] Wu J, Zhang L, Wang W, Su R, Gao X, Li S, Wang G and He R. 2023. Microstructures, mechanical properties and electromagnetic wave absorption performance of porous SiC ceramics by direct foaming combined with direct-ink-writing-based 3D printing. *Materials* **16**, 2861.
[138] Zhou N, Zhang L, Wang W, Zhang X, Zhang K, Chen M, Huang Y, He R and Fang D. 2023. Stereolithographically 3D printed SiC metastructure for ultrabroadband and high temperature microwave absorption. *Adv. Mater. Technol.* **8**, 2201222.
[139] Yang L, Wang L, Wang L, Liu G, Wang W, Zhang B and Tang X. 2025. Broadband, wide-angle, and high-temperature microwave absorbers enabled by 3D-printed torsion SiC metamaterials. *Thin-Walled Struct.* **214**, 113315.
[140] Wang W, Li Z, Gao X, Huang Y and He R. 2024. Material extrusion 3D printing of large-scale SiC honeycomb metastructure for ultra-broadband and high temperature electromagnetic wave absorption. *Addit. Manuf.* **85**, 104158.
[141] Meng Z, Li R, Zheng M, Yuan G, Zhou G, Guo J, Zhu X, Ren G and Li X. 2019. Fabrication and electromagnetic wave absorption performance of quartz ceramics containing inductive SiC screens. *Ceram. Int.* **45**, 13561–13566.
[142] Su R, Liu P, Chen J, Wang W, Chen X, He R and Li Y. 2025. Self-assembly and 3D printing of SiCw@MXene/SiOC metastructure toward simultaneously excellent terahertz electromagnetic interference (EMI) shielding and electron-to-thermal conversion properties. *Adv. Funct. Mater.* **35**, 2500970.
[143] Lv X, Ye F, Cheng L and Zhang L. 2022. 3D printing "wire-on-sphere" hierarchical SiC nanowires/SiC whiskers foam for efficient high-temperature electromagnetic wave absorption. *J. Mater. Sci. Technol.* **109**, 94–104.
[144] Mei H, Yang W, Zhao X, Yao L, Yao Y, Chen C and Cheng L. 2021. In-situ growth of SiC nanowires@carbon nanotubes on 3D printed metamaterial structures to enhance electromagnetic wave absorption. *Mater. Des.* **197**, 109271.
[145] Wang C, Tang J, Wang Z, She Y, Huang Z and Yang Y. 2024. Tuning the microstructure of porous SiCnw/SiC fabricated by vat photopolymerization 3D printing for electromagnetic wave absorption. *Ceram. Int.* **50**, 7745–7757.
[146] Terrani K A, Lach T, Wang H, Coq A L, Linton K, Petrie C, Koyanagi T and Byun T S. 2021. Irradiation stability and thermomechanical properties of 3D-printed SiC. *J. Nucl. Mater.* **551**, 152980.
[147] Petrie C M, Linton K D, Vasudevamurthy G, Schappel D, Seibert R L, Carpenter D, Nelson A T and Terrani K A. 2023. Fission gas retention of densely packed uranium carbonitride tristructural-isotropic fuel particles in a 3D printed SiC matrix. *J. Nucl. Mater.* **580**, 154419.
[148] Schappel D, Linton K D, Helmreich G W, Keever T J and Petrie C M. 2023. Failure analysis of nuclear transient-tested UN tristructural isotropic fuel particles in a 3D printed SiC matrix. *J. Nucl. Mater.* **586**, 154691.
[149] Wang Y, Liu H, Mei D and Yu S. 2022. Direct ink writing of 3D SiC scaffold as catalyst support for thermally autonomous methanol steam reforming microreactor. *Renew. Energy* **187**, 923–932.
[150] Heisel C, Caliot C, Chartier T, Chupin S, David P and Rochais D. 2021. Digital design and 3D printing of innovative SiC architectures for high temperature volumetric solar receivers. *Sol. Energy Mater. Sol. Cells* **232**, 111336.

[151] Yang J-J, Song Y-B, Li Z-H, Wang L-W, Shang S, Li H-K, Zhang H-C, Wang R, Lan H-B and Zhu X-Y. 2025. Structural design and simulation of PDMS/SiC functionally graded substrates for applications in flexible hybrid electronics. *Adv. Manuf.* **13**, 413–429.
[152] Guo Z, An L, Khuje S, Chivate A, Li J, Wu Y, Hu Y, Armstrong J, Ren S and Zhou C. 2022. 3D-printed electrically conductive silicon carbide. *Addit. Manuf.* **59**, 103109.
[153] Zhang Y, Cheng Y, Fang J, Ma D, Sun X, Li J, An Y, Hu N and Zhao L. 2025. 3D printing of (Cf-Csf)/ZrB2-SiC composites through coextrusion of flexible pre-infiltrated Cf/ZrB2 fiber bundle and Csf/ZrB2 paste. *Ceram. Int.* **51**, 31047–31058.
[154] Wang P et al. 2025. Photopolymerization and reaction sintering of ZrC/SiC ultra-high-temperature ceramics fabricated by 3D printing. *Ceram. Int.* **51**, 24583–24595.
[155] Zhang H, Wu H, Wang X, Gao A, Gong L, Zeng S, Li S, Liu M and Chen Y. 2025. Friction and wear behavior of 3D printed graphite/SiC composite self-lubricating materials with multi-materials and structures. *Tribol. Int.* **204**, 110487.
[156] Xiao S, Mei H, Han D, Yuan W and Cheng L. 2018. Porous (SiCw-Si3N4w)/(Si3N4-SiC) composite with enhanced mechanical performance fabricated by 3D printing. *Ceram. Int.* **44**, 14122–14127.
[157] Koyanagi T, Terrani K, Harrison S, Liu J and Katoh Y. 2021. Additive manufacturing of silicon carbide for nuclear applications. *J. Nucl. Mater.* **543**, 152577.
[158] Pelanconi M, Colombo P and Ortona A. 2021. Additive manufacturing of silicon carbide by selective laser sintering of PA12 powders and polymer infiltration and pyrolysis. *J. Eur. Ceram. Soc.* **41**, 5056–5065.
[159] Pelanconi M, Bianchi G, Colombo P and Ortona A. 2022. Fabrication of dense SiSiC ceramics by a hybrid additive manufacturing process. *J. Am. Ceram. Soc.* **105**, 786–793.
[160] Pelanconi M, Bottacin S, Bianchi G, Koch D, Colombo P and Ortona A. 2024. High-strength Si–SiC lattices prepared by powder bed fusion, infiltration-pyrolysis, and reactive silicon infiltration. *J. Am. Ceram. Soc.* **107**, 4436–4450.
[161] Pelanconi M et al. 2026. TPMS SiC structures produced by chemical vapour infiltration of SiC preforms shaped by powder bed fusion and binder jetting: a preliminary study on the early stages of the CVI process. *J. Eur. Ceram. Soc.* **46**, 117809.
[162] Ortona A, D'angelo C, Gianella S and Gaia D. 2012. Cellular ceramics produced by rapid prototyping and replication. *Mater. Lett.* **80**, 95–98.
[163] Dong S, Katoh Y and Kohyama A. 2003. Preparation of SiC/SiC composites by hot pressing, using tyranno-SA fiber as reinforcemen. *J. Am. Ceram. Soc.* **86**, 26–32.
[164] Zhang J, Jiang D, Lin Q, Chen Z and Huang Z. 2015. Properties of silicon carbide ceramics from gelcasting and pressureless sintering. *Mater. Des.* **65**, 12–16.
[165] Song N, Zhang H-B, Liu H and Fang J Z. 2017. Effects of SiC whiskers on the mechanical properties and microstructure of SiC ceramics by reactive sintering. *Ceram. Int.* **43**, 6786–6790.
[166] Mao F, Huang X, Ma X, Yang X, Zhang X and Yan Q. 2023. Microstructure evolutions of SiC whiskers at high temperature and its effects on silicon carbide ceramics. *Ceram. Int.* **49**, 29584–29594.
[167] Liu T, Yang L, Chen Z, Yang M and Lu L. 2023. Effects of SiC content on the microstructure and mechanical performance of stereolithography-based SiC ceramics. *J. Mater. Res. Technol.* **25**, 5184–5195.
[168] Song Z, Yang W, Hou Y, Zhang L, Zhang R, Dong Z, Huang X, Guo L, Jiang M and Ma Y. 2025. Binder jetting 3D printing preparation of SiC ceramics with low free silicon content and densification by PIP and LSI process. *J. Mater. Res. Technol.* **36**, 5899–5910.
[169] Feng K, Hu S, Li L, Mao Y, Heng Y, Yuan J, Wu J and Wei Q. 2023. Preparation of low residual silicon content Si-SiC ceramics by binder jetting additive manufacturing and liquid silicon infiltration. *J. Eur. Ceram. Soc.* **43**, 5446–5457.
[170] Zhong T, Lei L, Zhang Z, Hu D and Zhang J. 2024. Preparation of high-strength silicon carbide by SLS-RS. *Mater. Sci. Eng.* **914**, 147114.
[171] Gong L et al. 2025. Friction and wear properties of graphite/SiC composites built by SLS. *Tribol. Int.* **206**, 110589.
[172] Huang L, Chen R, Li S, Lao D, Jia W and Mao A. 2024. Microstructure and mechanical properties of continuous carbon fiber-reinforced SiC ceramic composite fabricated by direct ink writing. *Ceram. Int.* **50**, 25679–25688.
[173] Wang W, Bai X, Zhang L, Jing S, Shen C and He R. 2022. Additive manufacturing of Csf/SiC composites with high fiber content by direct ink writing and liquid silicon infiltration. *Ceram. Int.* **48**, 3895–3903.
[174] Wang G, Miao Y, Gong H, Sheng M, Jing J, Liu M, Lu J, Gong Z and Ma K. 2023. Direct ink writing of reaction bonded silicon carbide ceramics with high thermal conductivity. *Ceram. Int.* **49**, 10014–10022.
[175] Xu H, Liu Y and Wang K. 2024. Preparation high-performance SiC ceramic reinforced with 3D hybrid graphene oxide-carbon nanotube by direct ink writing and liquid silicon infiltration. *J. Eur. Ceram. Soc.* **44**, 5612–5622.
[176] Dong H, Qin S, Xie H, Liu P, Liu Z and Yang X. 2025. Application of compound carbon sources in additive manufacturing of high strengths reaction bonded SiC ceramics by fused deposition modeling method. *J. Eur. Ceram. Soc.* **45**, 117675.
[177] Liu Z, Li Z, Li Q, Wang C, Chen P, Yang L, Zhang L, Su B, Yan C and Shi Y. 2025. Ultra-High strength and toughness continuous SiCf/SiC ceramic matrix composites prepared by an additive manufacturing manipulator. *J. Eur. Ceram. Soc.* **45**, 117176.
[178] Wang W, Gao X, Li Z, Shen C, Ren X and He R. 2024. High performance Csf/SiC ceramic matrix composites fabricated by material extrusion 3D printing and precursor infiltration and pyrolysis. *Ceram. Int.* **50**, 44511–44520.
[179] Macdonald N P, Cabot J M, Smejkal P, Guijt R M, Paull B and Breadmore M C. 2017. Comparing microfluidic performance of three-dimensional (3D) printing platforms. *Anal. Chem.* **89**, 3858–3866.
[180] KOCEL AJS 2500. (available at: www.kocel.com/page16?product_id=287).
[181] Materialise 2025 Stereolithography. (available at: www.materialise.com/en/industrial/3d-printing-technologies/stereolithography).
[182] Materialise. 2025. Selective laser sintering. (available at: www.materialise.com/en/industrial/3d-printing-technologies/selective-laser-sintering).
[183] COBOD. 2025. 3D construction printer. (available at: https://cobod.com/solution/).
[184] Nanoscribe. 2025. Quantum X shape. (available at: www.nanoscribe.com/en/products/quantum-x-shape/#tab-43721).
[185] Fu H Z. 1998. Challenge and developement trends to future aero engine materials. *J. Aeronaut. Mater.* **18**, 54–63. (in Chinese)
[186] He X, Wang R, Qi S, Cheng J, Ye H, Li H, Chen S, Jian B and Ge Q. 2023. Vat photopolymerization 3D printing of polymer-derived SiOC ceramics with high precision and high strength. *Addit. Manuf.* **78**, 103889.
[187] Su R, Chen J, Zhang X, Gao X, Wang W, Li Y and He R. 2023. Accuracy controlling and mechanical behaviors of

precursor-derived ceramic SiOC microlattices by projection micro stereolithography (PμSL) 3D printing. *J. Adv. Ceram.* **12**, 2134–2147.

[188] Schmidt J, Brigo L, Gandin A, Schwentenwein M, Colombo P and Brusatin G. 2019. Multiscale ceramic components from preceramic polymers by hybridization of vat polymerization-based technologies. *Addit. Manuf.* **30**, 100913.

[189] Tan M, Cao J, Zhao S, Huang L, Zhang H, Liu M, Jia Z, Zhai R, Lu Z and Liu H. 2022. Cross-scale and cross-precision structures/systems fabricated by high-efficiency and low-cost hybrid 3D printing technology. *Addit. Manuf.* **59**, 103169.

[190] Jeong H, Cui Y, Tentzeris M M and Lim S. 2020. Hybrid (3D and inkjet) printed electromagnetic pressure sensor using metamaterial absorber. *Addit. Manuf.* **35**, 101405.

[191] Cheng J, Yu S, Wang R and Ge Q. 2024. Digital light processing based multimaterial 3D printing: challenges, solutions and perspectives. *Int. J. Extreme Manuf.* **6**, 042006.

[192] Wei C, Gu H, Zhang X, Chueh Y-H and Li L. 2020. Hybrid ultrasonic and mini-motor vibration-induced irregularly shaped powder delivery for multiple materials additive manufacturing. *Addit. Manuf.* **33**, 101138.

[193] Sajadi S M et al. 2021. Damage-tolerant 3D-printed ceramics via conformal coating. *Sci. Adv.* **7**, eabc5028.

[194] Sun J, Yu S, Wade-zhu J, Chen X, Binner J and Bai J. 2022. 3D printing of layered ceramic/carbon fiber composite with improved toughness. *Addit. Manuf.* **50**, 102543.

[195] Wang Y, Xu C, Liu J, Pan H, Li Y and Mei D. 2022. Acoustic-assisted 3D printing based on acoustofluidic microparticles patterning for conductive polymer composites fabrication. *Addit. Manuf.* **60**, 103247.

[196] Sun C, Huang Y, Wang W, Wang W, Pan W, Zong P, Yang L, Xing Y and Wan C. 2020. Embedding two-dimensional graphene array in ceramic matrix. *Sci. Adv.* **6**, eabb1338.

[197] Wang W, Gao X, Zhang L, Ma Q, Li S, Li Z, Shen C, Wang G and He R. 2023. Large-scale material extrusion-based additive manufacturing of short carbon fibre-reinforced silicon carbide ceramic matrix composite preforms. *Virtual Phys. Prototyp.* **18**, e2245801. (In German)